International Journal of Nanomedicine

Dovepress
open access to scientific and medical research

Open Access Full Text Article

ORIGINAL RESEARCH

Human Keratinocyte-Derived Exosomal MALAT1 Promotes Diabetic Wound Healing by Upregulating MFGE8 via microRNA-1914-3p

Liwen Kuang[1,*], Chenchen Zhang[1,*], Binghui Li[1], Haibo Deng[1], Ran Chen[1], Gongchi Li[2]

[1]Department of Wound Repair Surgery, Liyuan Hospital, Tongji Medical College, Huazhong University of Science and Technology, Wuhan, Hubei, 430062, People's Republic of China; [2]Department of Hand Surgery, Union Hospital, Tongji Medical College, Huazhong University of Science and Technology, Wuhan, Hubei, 430022, People's Republic of China

*These authors contributed equally to this work

Correspondence: Gongchi Li, Department of Hand Surgery, Union Hospital, Tongji Medical College, Huazhong University of Science and Technology, No. 1277 Jiefang Road, Wuhan, Hubei, 430022, People's Republic of China, Tel +8613618615209, Email ligongchi@foxmail.com

Purpose: Diabetic wound is a highly prevalent and refractory disease. Extensive studies have confirmed that keratinocytes and macrophages play an important role in the process of wound healing. Additionally, exosomes are regarded as a vital intercellular communication tool. This study aimed to investigate the role of human keratinocyte-derived exosomal MALAT1 in the treatment of diabetic wound by influencing the biological function of macrophages.

Methods: We mainly assessed the function of MALAT1 on the biological changes of macrophages, and the expression of MALAT1 in the keratinocyte-exosomes analyzed by quantitative real-time polymerase chain reaction (RT-qPCR). The downstream interaction between RNAs or proteins was assessed by mechanistic experiments. Besides, we evaluated the effects of human keratinocyte-derived exosomal MALAT1 on diabetic wound healing in vivo to verify in vitro results.

Results: We demonstrated that human keratinocyte-derived exosomal MALAT1 enhanced the biological functions of high glucose-injured macrophages, including phagocytosis, converting to a pro-healing phenotype and reducing apoptosis. Mechanistically, MALAT1 accelerated the expression of MFGE8 by competitively binding to miR-1914-3p, thereby affecting the function of macrophages and the signal axis of TGFB1/SMAD3, and finally promoting the healing of diabetic wounds. Human keratinocyte-derived exosomal MALAT1 might promote collagen deposition, ECM remodeling, and expression of MFGE8, VEGF, and CD31 but reduce the expression of TGFB and SMAD3 in an in vivo model of diabetic mice wounds, which accelerated diabetic wound healing and restored its function.

Conclusion: The current study revealed that human keratinocyte-derived exosomal MALAT1 would suppress miR-1914-3p to activate MFGE8 and eventually promote wound healing by enhancing macrophage phagocytosis, converting to a pro-healing phenotype and reducing apoptosis. It proposed that keratinocyte-derived exosomes might have the capacity to serve as a new method for the clinical treatment of diabetic wound.

Keywords: exosomes, keratinocytes, macrophages, MALAT1, diabetic wound healing

Introduction

Diabetic intractable wounds have a lifetime prevalence of 25% among people with diabetes and a 3-year mortality rate of 35–65% worldwide.[1] Peripheral neuropathy and vasculopathy due to chronic hyperglycemia are the leading causes of poor wound healing.[2] The standard treatment for diabetic wounds remains surgical debridement, dressing and improvement of circulation, blood sugar and infection.[3] Adjunctive treatments such as oxygen administration, negative pressure wound therapy, cell-free biologics and human growth factors are also being used.[4] However, with these comprehensive treatments, we must acknowledge that the incidence of delayed diabetic wound healing remains high. The molecular mechanisms underlying the delayed repair of diabetic wounds have been well studied. Still, there are no practical

Received: 6 January 2023
Accepted: 14 February 2023
Published: 21 February 2023

Graphical Abstract

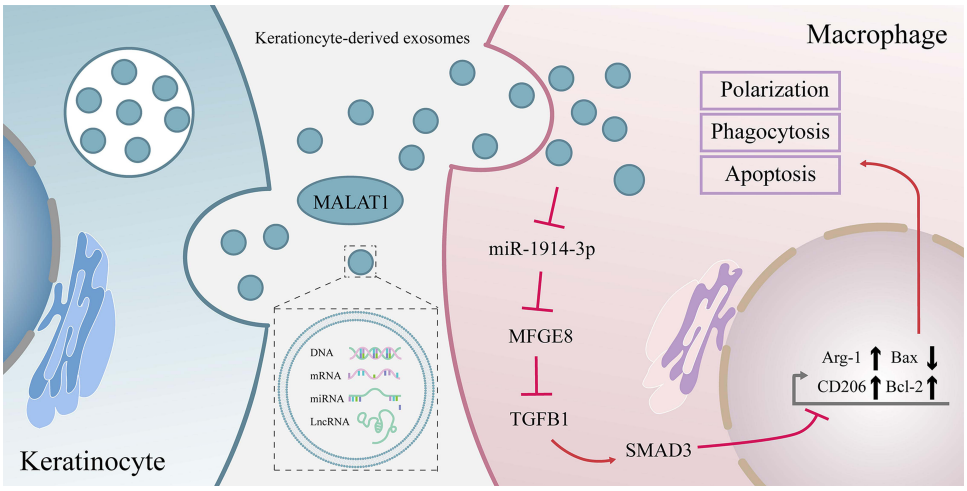

clinically targeted therapeutic approaches to promote wound repair by influencing molecular mechanisms. Therefore, searching for a new mechanism to encourage the process of wound repair is vital for the targeted promotion of poor healing wound repair.

Several studies have identified multiple differentially expressed long non-coding RNA (lncRNAs) in diabetic wounds compared to non-diabetic wounds,[5] metastasis-associated lung adenocarcinoma transcript 1 (MALAT1) being one of them. MALAT1 can act as a competing RNA and bind to various microRNAs(miRNAs) to exert biological functions. For example, MALAT1 can bind to miR-1914-3p[6] to increase YAP activity and induce NSCLC drug resistance and metastasis. It combined with miR-124[7] or miR-378a[8] to promote wound healing, and miR-142-3p[9] to accelerate endometrial stromal cell proliferation and inhibit cell apoptosis.

MiRNA is a short non-coding RNA about 22nt long, which typically inhibits messenger RNA (mRNA) translation at the post-transcriptional level by binding to the mRNA 3'untranslated region(3'UTR).[10] In our previous study, we found that is a potential target gene of miR-1914-3p, milk fat globule EGF and factor V/VIII domain containing (MFGE8). And knocking out MFGE8 in mice will increase the inflammatory response and slow wound healing.[11] MFGE8 is a secreted glycoprotein that interacts with macrophages and binds to αvβ3-integrin and phosphorylated serine sites, respectively. It also plays an essential role in promoting macrophage phagocytosis,[12] polarization[13] and reducing apoptosis and organ damage.[14]

Previous studies have confirmed that exosomes can act as a messenger to link keratinocytes (KCs) and macrophages in both directions.[15] Meanwhile, several studies have demonstrated that lncRNA carried in exosomes can promote wound healing. For example, lncRNA H19-containing MSC-derived exosomes prevent fibroblast apoptosis and inflammation via the miR-152-3p/PTEN axis.[16] Adipose-derived stem cell-derived exosomes containing MALAT1 target miR-124 and activate the Wnt/β-catenin pathway to promote proliferation, migration and inhibit apoptosis in HaCaT and HDF cells.[7] In recent years, with the advancement of technology, efficient and inexpensive exosome extraction techniques have become more sophisticated, making exosomes an excellent candidate vehicle for targeted treatment of diabetic wound.[17]

Modification of exosomes using the process of exosome biogenesis or with the help of techniques such as electroporation, co-incubation, repeated freeze-thawing, ultrasound, extrusion, and surface modification is an effective way to enhance the biological activity of exosomes and improve their therapeutic effects.[18] For example, dendritic exosomes was modified with a fusion peptide of exosomal membrane protein (Lamp2b) and neuron-specific RVG3 peptide and loaded with siRNA by electroporation, giving them the ability to target delivery of siRNA.[19] Another study constructed a fusion gene plasmid vector for Lamp2b and muscle-specific targeting peptide and cotransfected it with adenovirus

expressing miR-26a to produce exosomes targeting muscle highly expressing miR-26a. Tail vein such exosomes will ameliorate the muscle wasting and cardiomyopathy that occurs in chronic kidney disease mice.[20]

The above study illustrates that we can improve exosomes to make them highly express MALAT1 and thus have a pro-wound healing function. However, the contribution of exosomes with high expression of MALAT1 from keratinocyte HaCat to wound healing has not been demonstrated so far. Therefore, this project aimed to investigate whether exosomes from keratinocytes with high expression of MALAT1 could enhance the biological properties of macrophages and thus contribute in the promotion of diabetic wound healing. In addition, we further investigated whether MALAT1 worked through the MALAT1/miR-1914-3p/MFGE8 signaling axis in the healing process of diabetic wounds to provide new possibilities for the clinical targeting of diabetic wounds.

Materials and Methods

Establishment of a Mouse Model

Healthy male C57BL/6 mice (6 weeks old) were housed at a constant temperature and humidity, with a 12:12-h light-dark cycle. After 1 week of adaptive feeding, part of the mice was randomly selected as the normal control group by injecting normal saline with normal feeding. The remaining mice were used to establish diabetic models by feeding with a high-glucose and high-fat diet for 4 weeks and intraperitoneally injected with 0.45% streptozotocin (STZ; 45 mg/kg). After seven days, the tail blood glucose level was measured by a blood glucose meter. Mice with a blood glucose level higher than 16.7 mM continuously for three days were enrolled in our study.

The macrophage depletion was conducted following the instructions. 0.2 mL of Clodronate liposomes (LIPOSOMA, Netherlands) or PBS liposomes were injected intraperitoneally every three days per 20 g of adult mice.[21,22] Immunohistochemical staining analysis was performed on day 7 after the first injection to evaluate the efficacy of macrophage depletion. Briefly, liver and spleen tissue were stained with F4/80 on paraffin slides. The presence of resident macrophages was determined by F4/80 positive cells, and the positive cells were reduced by 80% compared to the control group, demonstrating the overall success of macrophage depletion.

The first step in creating a wound model is narcotising mice with 4% isofluorane, which is maintained by 2%. Then the dorsal area of the mice was shaved. Full-thickness wounds (10 mm diameter) were made on the back using a sterile punch, and a 1 cm round silicone ring was sutured around the damage to avoid contraction. 200 μL of exosomes (1 mg/mL), including KC-Exo vector and KC-Exo carrying oe-MALAT1, were injected subcutaneously into the skin around the wound (four sites for each) at 0, 3, 7, and 14 days, respectively.[23–27] The control group was injected with an equal volume of saline solution. The wound-healing area was assessed. Wound tissues and surrounding areas were harvested 0, 3, 7, 14, and 21 days after the procedure. The wound healing rate was calculated as follows: The healing rate = (Area of initial wound − Area of the residual wound) / Area of initial wound×100%.

Histology

The tissues were fixed in 10% paraformaldehyde for at least 24 h, and then embedded in paraffin. Paraffin-embedded tissue samples were cut into 2–3 μm sections, deparaffinised in xylene, dehydrated through a graded series of ethanol, stained with Haematoxylin-eosin (H&E) and Masson's trichrome (MT), and mounted in resin. The images were captured using an optical microscope.

Immunohistochemical

The paraffin-embedded sections were dehydrated by an ascending series of ethanol and washed with running water for 2 min. Then, the sections were immersed in 3% H_2O_2 for 20 min, followed by washing with distilled water for 2 min and 0.1 M PBS for 3 min. The samples were blocked by incubation in normal goat serum at room temperature for 20 min. Slides were incubated overnight at 4°C with the primary rabbit anti-mouse antibody to VEGF and CD31. Following incubation with the secondary goat anti-rabbit antibody to immunoglobulin G and horseradish peroxidase (HRP)-labelled streptavidin working solution at 37°C for 20 min, labelling was visualised using DAB with hematoxylin. The sections

were returned blue by adding 1% ammonia, then were dehydrated with gradient alcohol, cleared by xylene, and mounted with neutral resin. The area was observed and photographed under an optical microscope.

RNA Isolation and Quantitative Real-Time Polymerase Chain Reaction (RT-qPCR)

For RNA preparation, cultured cells and mice skin specimens were sorted into Trizol reagent (Invitrogen, USA), and RNA was obtained per the accompanying guidance. Later, complementary DNA (cDNA) was acquired by the reverse transcription of the extracted total RNA via the HiScript II Q RT SuperMix for qPCR (+gDNA wiper) (Vazyme, China). The cDNA was generated using miRNA 1st Strand cDNA Synthesis Kit (by stem-loop) (Vazyme, China). RT-qPCR with designed primers and ChamQ Universal SYBR qPCR Master Mix (Bio-Rad) was run in quadruplicate on a fluorescence ration PCR instrument. Results were normalised by the amount of β-actin or U6 expression and calculated based on the $2^{-\Delta\Delta Ct}$ formula.

Western Blot Analysis

For protein preparation, cultured cells and mice skin specimens (using a manual pestle homogeniser) were lysed in an appropriate volume of cold RIPA buffer plus protease inhibitors. BCA Kit (Beyotime, China) was used to measure protein concentration. Extracted protein (20 μg) was separated by SDS-polyacrylamide electrophoresis (SDS-PAGE) before being transferred onto polyvinylidene fluoride (PVDF) membranes. For immunodetection, primary antibodies specific for CD63(Abcam, UK), TSG101(Abcam, UK), MFGE8(Abcam, UK), Bax (Abcam, UK), Bcl-2(Abcam, UK), CD206(Abcam, UK), Arg-1 (Abcam, UK), iNOS (Abcam, UK), TGFB1 (Abcam, UK), SMAD3 (Abcam, UK) and GAPDH (Abcam, UK). IgG secondary antibody labelled by horseradish peroxidase (Abcam, UK), and enhanced chemiluminescence were used.

Cell Line and Reagent

The human skin keratinocyte cell line HaCaT, the human myeloid leukemia mononuclear cell line THP-1 and the human embryonic kidney cell line 293T were obtained from Procell Life Science &Technology, Wuhan, China. HaCaT was cultured in MEM medium (HyClone, Logan, UT, USA), THP-1 was cultured in RPMI 1640 medium (HyClone, Logan, UT, USA), and HEK293T was cultured in DMEM medium (Gibco, Grand Island, NY, USA), three of them containing 10% fetal bovine serum (FBS, Gibco, Grand Island, NY, USA). All cells were cultured in the specific media with 100 U/mL penicillin and 100 μg/mL streptomycin at 37°C with 5% CO_2. THP-1 cells were treated with phorbol myristate acetate (PMA, MCE, China) at 100 ng/mL for 24 hours to obtain THP-1-derived macrophages. The polarization model was successfully constructed by measuring the expression of CD11b and CD14 through WB. The matured M0 macrophages were treated with 20 ng/mL interferon (PEPROTECH, USA) and 100 ng/mL lipopolysaccharide (LPS, PEPROTECH, USA) 24h to produce M1 polarized macrophages, and converted into M2 macrophages by using the interleukin-4 and interleukin-13 (IL-4, IL-13, PEPROTECH, USA, 20ng/mL, respectively) treatments. For the cellular high glucose model, THP-1 cells were treated with D-(+)-Glucose (Sigma-Aldrich, USA) at 35 mmol/l concentration, and the cellular normal glucose model was treated with D-(+)-Glucose at 5.6 mmol/l concentration.

Transfection

MALAT1 cDNA and MFGE8 cDNA were synthesized and cloned into pcDNA3.1 plasmid for overexpression, and pcDNA3.1 plasmid containing a scrambled sequence was used as negative control (NC). SiRNA-MALTA1, siRNA-NC, MALAT1 plasmid, MFGE8 plasmid and empty vector plasmid were purchased from Gene Create (Wuhan, China). MiR-1914-3p mimics, mimics NC, miR-1914-3p inhibitor and inhibitor NC were all constructed by Ribo (Guangzhou, China). Before transfection, cells were seeded in six-well plates and grown in a specific medium with 10% fetal bovine serum for 24h in a humidified 37 °C incubator with 5% CO_2. Then siRNA, plasmid DNA, mimic or inhibitor was transfected into the cells using a Jetprime Polyplus Transfection Reagent (Polyplus-transfection SA, Illkirch, France) following the manufacturer's protocol.

Coculture of KCs or Exosomes and THP-1-Derived Macrophages

KCs were treated with an exosome inhibitor (GW4869) to inhibit the exosomal secretion of KCs. KCs were plated in a 6-well plate at 1×10^6 cells/well density. When the cells reached 80%–90% confluence, 10μM GW4869 was introduced to treat KCs. The cells and supernatant were harvested after 24 h for further use. KCs were plated on the 6-well basolateral chambers of a Transwell chamber at a density of 1×10^6 cells/well, whereas apical chambers were added with THP-1-derived macrophages. The insertion well size between the apical and basolateral chambers was 0.4 um. After coculture for 24h, the THP-1-derived macrophages were isolated, and the expression of miR-1914-3p and MFGE8 in each group was determined. THP-1-derived macrophages were cocultured with KCs, KCs+GW4869, KCs+oe-NC, KCs +oe-MALAT1, KCs+si-NC, and KCs+si-MALAT1, respectively.

Exosome Isolation and Characterization

KCs were cultured until 80%–90% confluence overnight in serum-free MEM and centrifuged at 2000 g for 20 min at 4°C to remove cell debris. The obtained supernatant was ultracentrifuged at 10,000 g for 1 h at 4°C. The pellet was suspended in PBS and submitted to another ultracentrifugation in the same conditions. The shot was stored at 80°C until further use. The identification of exosomes was confirmed by transmission electron microscopy (TEM, HITACHI), NTA, and Western blot. TEM was used to examine the morphology of exosomes, and NTA was applied to analyze the particle size of exosomes. The surface markers of exosomes (CD63, TSG101) were assessed by Western blot. The expression of MALAT1 in exosomes was determined by RT-qPCR. Exosomes were pooled together for each group for further cell and animal experiments

Bioinformatics Prediction

We searched the possible miRNAs that may be involved in crosstalk with 3'untranslated region (3'UTR) regions of MFGE8 by applying three different target prediction algorithms miWalk (http://mirwalk.umm.uni-heidelberg.de),[28] ENCORI (https://starbase.sysu.edu.cn/index.php)[29] and Targetscan (https://www.targetscan.org).[30] After identifying miR-1914-3p as the research target, the interaction between miR-1914-3p and the MALAT1 was predicted by RNA22 (https://cm.jefferson.edu/rna22/Interactive),[31] DIANA-LncBase (https://diana.e-ce.uth.gr/lncbasev3)[32] and ENCORI.

Luciferase Reporter Assay

Through the database mentioned above, we predicted that the segments of MALAT1 and MFGE8 3'UTR encompass the binding sites for miR-1914-3p. The MFGE8-WT (PmirGLO-MFGE8-WT) and MFGE8-Mut (PmirGLO- MFGE8-Mut) vectors, along with the MALAT1-WT (PGLO-MALAT1-WT) and MALAT1-MUT (PGLO-MALAT1-Mut) vectors were constructed by Gene Create (Wuhan, China). For the luciferase assay, HEK 293T cells seeded on 24-well culture dishes ($1x10^5$ cells/well) 24 h before transfection were co-transfected with the reporter vectors, miR-1914-3p mimic and mimic NC. After 48h of transfection, the cells were harvested, lysed, and centrifuged at 12,000 rpm for 10 min. The luciferase activity was measured using a Dual-Luciferase Reporter Assay Kit (Promega, USA) according to the manufacturer's instructions. Luciferase activity was normalized by the Firefly/Renilla luciferase signal in cells.

RNA-Immunoprecipitation (RIP)

The binding between MALAT1 and argonaute RISC catalytic component 2 (AGO2) was detected using a RIP kit (BersinBio, Guangzhou, China). The cells were lysed with an equal volume of polysome lysis buffer with protease inhibitor and RNase inhibitor in an ice bath for 10 min. After adding DNase to the cell lysate, the cells were bathed in a warm bath for 10min at 37°C, then centrifuged at 16,000 g for 10 min at 4°C, and the supernatant was then collected. A part of the cell extract was used as an input. In contrast, the rest were evenly divided into two parts, added protein A/G beads, and probed with AGO2 antibody (Abcam, Cambridge, UK) and IgG antibody (Abcam, Cambridge, UK) for a coprecipitation reaction, respectively. After protease K added, RNA was isolated from the sample, and then RT-qPCR was performed.

RNA Pull-Down Assay

Biotinylated miR-1914-3p(Bio-miR-1914-3p-WT), the matched mutants in the target region (Bio-miR-1914-3p-MUT), and the corresponding negative control (Bio-NC) were obtained from Gene Create (Wuhan, China). Cell lysates prepared with cold RIPA buffer were incubated with Bio-miR-1914-3p-WT, Bio-miR-1914-3p-MUT, or Bio-NC and streptavidin beads overnight at 4°C. Beads were harvested, and RNA bound to beads purifying by Trizol was prepared to measure the MALAT1 level by RT-qPCR.

Cellular Uptake of Exosomes in vitro

Following the recommended procedures, the exosomes of the isolated KCs were marked with DiI (red) (Invitrogen, USA). For 6, 12 or 24 hours, THP-1-derived macrophages and DiI-labeled exosomes were cocultured in confocal plates. After removing the cell medium with a third PBS wash, the cells were fixed for 30 minutes with 4% paraformaldehyde. The blue fluorescence dye DAPI labelled the cell nuclei (Invitrogen, USA). Fluorescence was seen with a laser scanning confocal microscope (OLYMPUS, Japan).

Cell Apoptosis Assay

Cell apoptosis was analyzed using Annexin V-PE/7-AAD Apoptosis Detection kit (Vazyme, Nanjing, China) 24h after transfection. Cells were centrifuged at 4°C at 1000 × g for 5 min to remove the supernatant. Cells were washed with PBS 2 times and counted. Subsequently, 5×10^5 cells were stained with 100 μL binding buffer, 5 μL Annexin V-PE and 5 μL 7-AAD staining solution. After incubation at room temperature in the dark for 10 min, cells were added 400μL binding buffer and mixed well. Apoptotic cells were examined by flow cytometry within one hour after staining. Data were analyzed by FlowJo 10.0 (FlowJo Software, USA).

Statistical Analysis

GraphPad Prism8 (GraphPad Software Inc; La Jolla, CA, USA) was applied for data analysis. The measurement data were expressed as mean ± SD. Our data were checked for normality test (Kolmogorov–Smirnov test) and homogeneity of variance (Fisher's F-test). Comparison between the two groups was conducted by Student's *t*-test. One-way ANOVA was used for data comparison among multiple groups, followed by Tukey's post hoc test. Repeated-measures two-way ANOVA was applied for data comparison among various groups at different time points, followed by Tukey's post hoc test. The correlation among lncRNA, miRNA and mRNA were analyzed by Spearman correlation analysis. Values of $p < 0.05$ were considered statistically significant.

Results

Macrophage Depletion Inhibited Wound Healing

As mentioned above, KCs and macrophages play important roles in wound repair. Clodronate liposomes, which kill macrophages, were injected into an STZ-induced diabetic model of C57BL/6J mice to confirm the effectiveness of wound macrophages in diabetic wound healing. We first tested the liposomal PBS's toxicity in vivo by intraperitoneally injecting normal mice with PBS or PBS liposomes. No discernible changes in skin structure levels and other cytokines were seen after 7 days of administration (Supplementary Figure 1A and B). Then, by the manufacturer's recommendations, diabetic mice received intraperitoneal administration of clodronate and control PBS liposomes. Immunohistochemical staining of F4/80-positive cells in the macrophages confirmed macrophage depletion. Immunohistochemical staining of F4/80-positive cells in the spleen and liver of mice provided evidence of the depletion of macrophages (Figure 1A and B). We found that the injection of clodronate liposomes significantly reduced the rate of wound healing in an STZ-induced diabetic mouse model of chronic wounds (Figure 1C and D). Histological analysis revealed that the group treated with clodronate liposomes had worse structural integrity, accompanied by a catastrophic loss of collagen fibers (Figure 1E and F). Additionally, in the repair phase, wound crypts in the clodronate liposome-treated group showed fewer CD31-positive cells and lower levels of VEGF expression than those in the control group (Figure 1G and H).

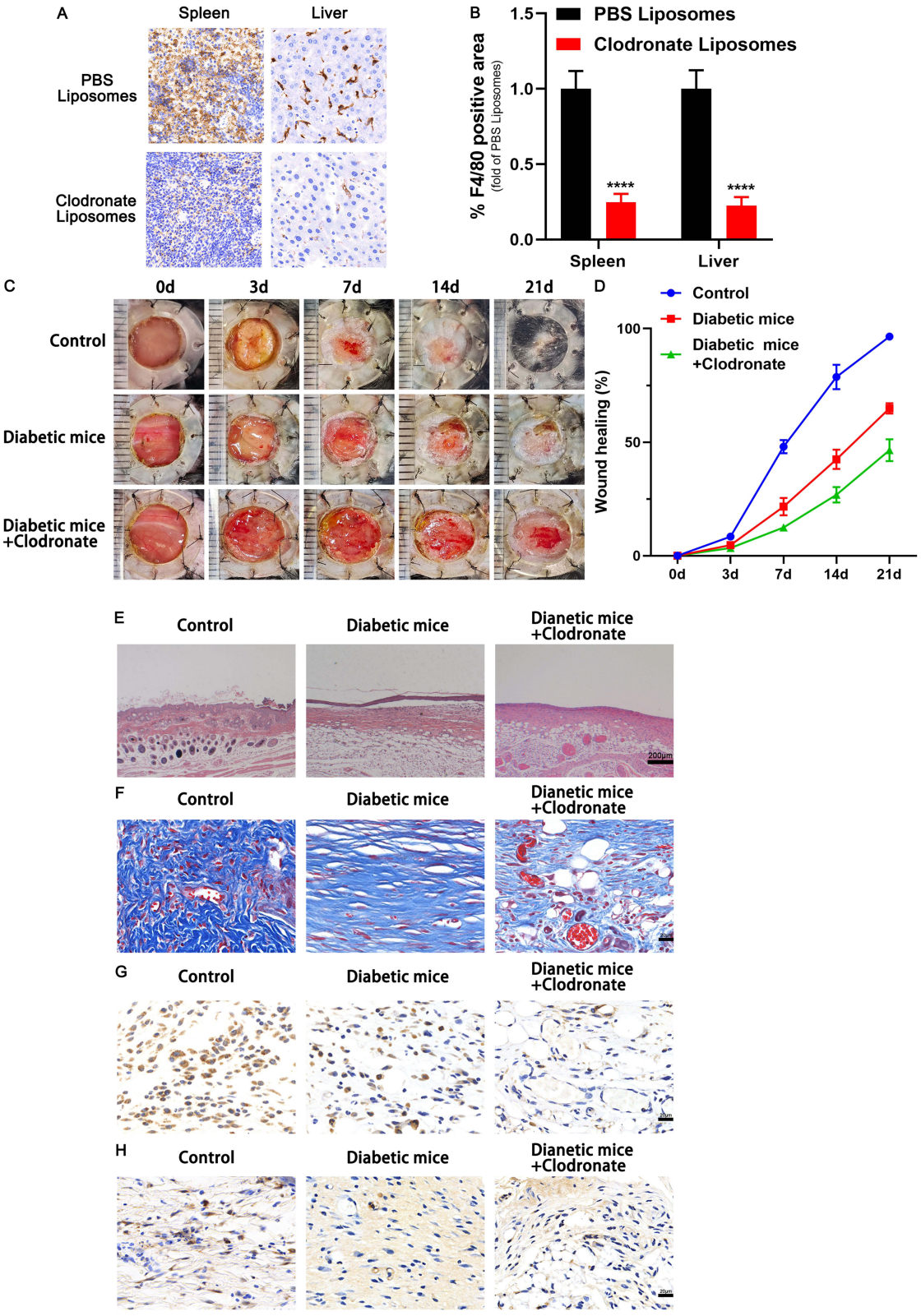

Figure 1 Macrophage depletion inhibited wound healing. (**A**) Efficiency of macrophage depletion in the liver and spleen of normal C57BL/6 mice. F4/80-positive cells were analysed by immunohistochemical staining. (**B**) Quantitative analysis of the F4/80-positive cells in the two groups. (**C**) Representative images of full thickness defects in mice receiving treatment with PBS (Control), STZ (Diabetic mice) and STZ+ Clodronate Liposomes (Diabetic mice+ Clodronate) at days 0, 3, 7, 14, and 21 days postoperatively. (**D**) Wound healing closure rates was calculated among the different groups using the ImageJ software. (**E**) HE staining among the different groups at day 14, Scale bar: 200μm. (**F**) Masson's trichrome staining and quantification of collagen fiber at day 14, Scale bar: 20μm. (**G**) Representative immunohistochemical images of CD31, Scale bar: 20μm. (**H**) Representative immunohistochemical images of VEGF, Scale bar: 20μm. ****p < 0.0001 versus the PBS Liposomes group (n = 5). Measurement data were expressed as mean ± SD. Comparison between two groups was conducted using independent sample *t* test.

https://doi.org/10.2147/IJN.S399785 DovePress

MiR-1914-3p Targeted MFGE8 to Affect Macrophage Phagocytosis, Apoptosis, and Polarization via the TGFB1/SMAD3 Signaling Pathway

Previous studies illustrate that miRNA and MFGE8 are expressed differently in diabetic wound skin and normal tissue.[33,34] To further elucidate the molecular mechanism of MFGE8 in promoting wound repair, we first examined the expression of miR-1914-3p and MFGE8 in THP-1-derived macrophages cultured under low and high glucose conditions, as well as in the peri-wound skin tissues of normal mice and type 2 diabetic mice, respectively, using RT-qPCR. The results showed that miR-1914-3p expression was significantly higher in THP-1-derived macrophages cultured with a high glucose medium and MFGE8 expression was significantly lower in peri-traumatic tissues of diabetic mice in a high glucose environment (Figure 2A-C). We further analyzed the correlation between miR-1914-3p and MFGE8, and as shown in Figure 2D, the expression of miR-1914-3p and MFGE8 in 31 peritraumatic tissues was negatively correlated. The MFGE8 3'UTR region was predicted to contain a potential binding site for miR-1914-3p according to the ENCORI, TargetScan and miRWalk databases (Figure 2E and F). To further verify the above speculation, we performed a luciferase reporter gene assay by co-transfecting plasmids constructed with MFGE8-WT or MFGE8-MUT and miR-1914-3p mimic or mimic-NC into HEK293T cell lines. The results showed that MFGE8-WT luciferase activity was attenuated in the miR-1914-3p mimic group compared to the mimic-NC group. In contrast, there was no significant difference in the luciferase activity of MFGE8-MUT, suggesting that miR-1914-3p specifically binds MFGE8 3'UTR (Figure 2G).

RT-qPCR and Western blot analysis showed that the presence of miR-1914-3p mimic significantly reduced MFGE8 mRNA and protein expression in THP-1-derived macrophages compared to THP-1-derived macrophages transfected with mimic-NC. An opposite trend was observed in miR-1914-3p inhibitor-treated THP-1-derived macrophages compared to inhibitor-NC treatment, and THP-1-derived macrophages co-transfected with miR-1914-3p mimic and oe-MFGE8 showed no significant difference, which indicates that MFGE8 was negatively regulated by miR-1914-3p ((Figure 2H, N and O). Subsequently, we investigated the regulatory effects of miR-1914-3p and MFGE8 on THP-1-derived macrophages' phagocytosis, apoptosis and polarization. As part of this experiment, THP-1 cells were analyzed for the expression of CD11b and CD14 by Western blot to confirm the successful polarization of non-polarized macrophages (M0) (Supplementary Figure 2). The results showed that miR-1914-3p inhibitor or oe-MFGE8 treatment promoted macrophage phagocytosis (Figure 2I and J and Supplementary Figure 3A) and inhibited apoptosis (Figure 2K and L), while RT-qPCR and WB verified that Bcl-2 expression was increased and Bax expression was downregulated (Figure 2M-O). After THP-1-derived macrophages were polarized to M1 and M2, respectively, the protein expression of iNOS, Arg-1 and CD206 was detected by WB. M1-polarized THP-1 macrophages were found to have high expression of iNOS and low expression of Arg-1 and CD206, and M2-polarized THP-1 macrophages had the opposite trend (Supplementary Figure 4), indicating that we can assess the polarization direction by the detection of the above three indicators. The miR-1914-3p inhibitor or oe-MFGE8 also reduced the expression of M1 macrophage marker iNOS and increased the expression of M2 macrophage markers Arg-1 and CD206, while miR-1914-3p mimic and si-MFGE8 showed the opposite trend (Figure 2M-O). MFGE8 is an essential inhibitor of the TGFB1/SMAD3 signaling pathway. It plays a vital role in mediating phagocytosis, apoptosis, polarization and glucose metabolism in macrophages. We hypothesised that the above phenomenon might be achieved through the TGFB1/SMAD3 signaling pathway. RT-qPCR and WB were performed to determine the expression of TGFB1 and SMAD3. The results showed that the expression of TGFB1 and SMAD3 was significantly reduced in macrophages treated with miR-1914-3p inhibitor or oe-MFGE8, while the opposite was true for miR-1914-3p mimic and si-MFGE8 treatment (Figure 2M-O). This suggests that MFGE8 3'UTR binding by miR-1914-3p can alter TGFB1 and SMAD3 expression. Taken together, these findings clarify that miR-1914-3p inhibits phagocytosis of macrophages by regulating MFGE8, promotes their conversion to the M1 type, and induces apoptosis.

MALAT1 Competitively Bound to miR-1914-3p to Inhibit the Activity of the TGFB1/SMAD3 Signaling Pathway and Affect Macrophage Phagocytosis, Apoptosis, and Polarization

It has been shown that lncRNA can act as ceRNA to regulate miRNA expression. We hypothesised that ceRNA is a possible mechanism by which MFGE8 is regulated during trauma repair. To further elucidate the above tool, we first used RT-qPCR to detect MALAT1 expression in THP-1-derived macrophages cultured under low and high glucose conditions and in periwound

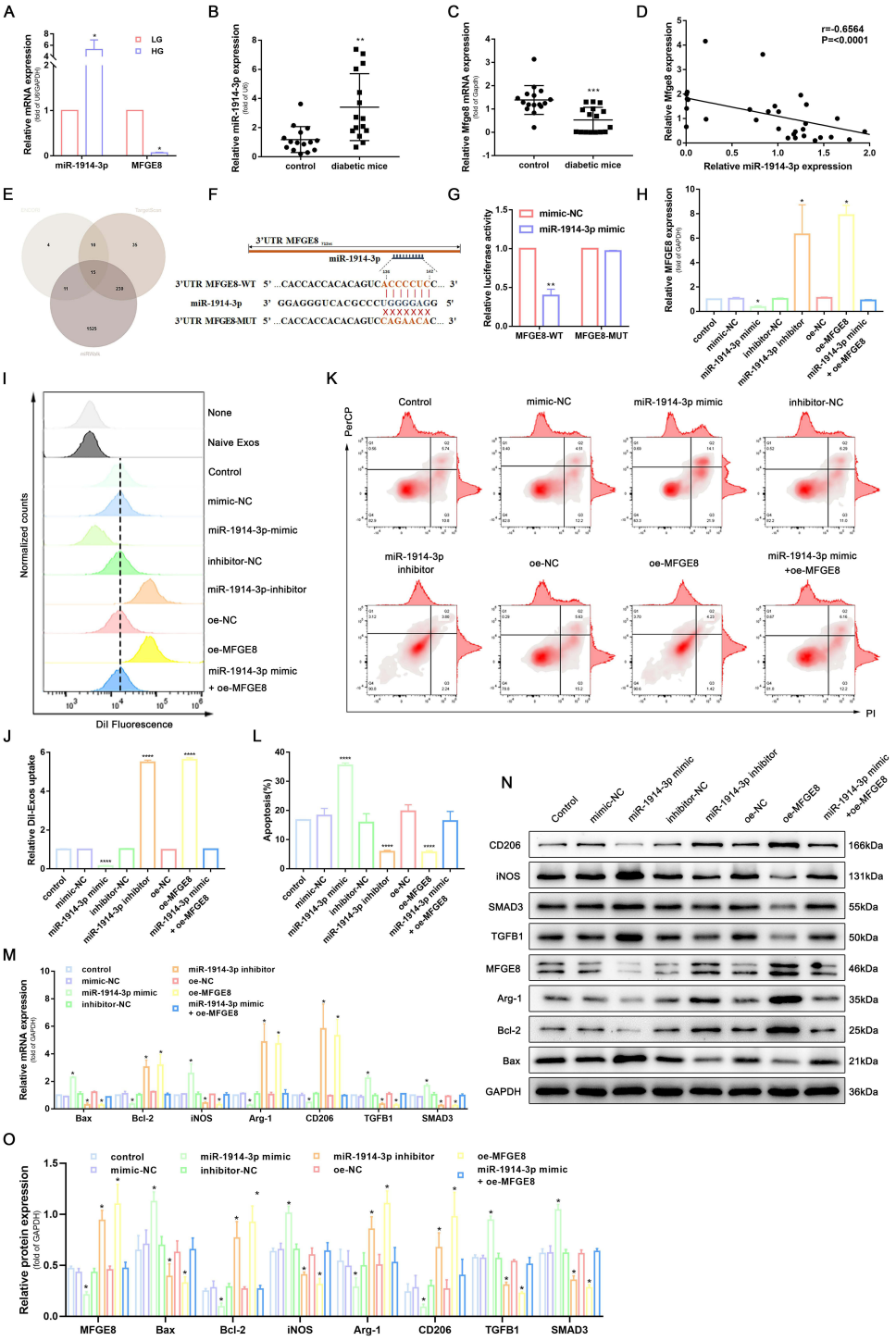

Figure 2 MiR-1914-3p targeted MFGE8 to affect macrophage phagocytosis, apoptosis, and polarization via the TGFB1/SMAD3 signaling pathway. (**A**) miR-1914-3p expression and mRNA expression of MFGE8 in THP-1-derived macrophages under a normal medium or high glucose medium, determined by qRT-PCR. (**B** and **C**) miR-1914-3p expression and mRNA expression of MFGE8 in wound tissue from normal mice or diabetic mice, determined by qRT-PCR. (**D**) The correlation between miR-1914-3p and MFGE8 expression, measured in 31 mice skin by Spearman correlation analysis. (**E**) Predicted target miRNAs of MFGE8 by three online databases (ENCORI, TargetScan and miRWalk). (**F**) Predicted binding sites between miR-1914-3p and MFGE8 by bioinformatics database. (**G**) Luciferase activity of MFGE8-WT and MFGE8-MUT detected by dual-luciferase reporter gene assay. (**H**) mRNA expression of MFGE8, determined by qRT-PCR. (**I** and **J**) Uptake of DiI-labelled KCs-Exo by PMA-treated THP-1 cells, measured by flow cytometry analysis. (**K** and **L**) Apoptosis in PMA-treated THP-1 cells, measured by flow cytometry analysis. (**M**) mRNA expression of apoptosis-related factors (Bax and Bcl-2), macrophage polarization-related surface markers (iNOS, Arg-1 and CD206), TGFB1 and SMAD3, determined by qRT-PCR. (**N** and **O**) Protein expression of apoptosis-related factors (Bax and Bcl-2), macrophage polarization-related surface markers (iNOS, Arg-1 and CD206), MFGE8, TGFB1 and SMAD3, normalized to GAPDH, determined by Western blot analysis. *p < 0.05, **p < 0.01, ****p < 0.0001 versus the control group. Measurement data were expressed as mean ± SD. Comparison between two groups was conducted using independent sample *t* test. One-way ANOVA was used for data comparison among multiple groups, followed by Tukey's post hoc test. The experiment was repeated independently three times.

skin tissues of ordinary and type 2 diabetic mice. The results showed that MALAT1 expression was significantly reduced in THP-1-derived macrophages in the high glucose environment and peri-traumatic tissues of diabetic mice (Figure 3A and B). We further analysed the correlation between MALAT1 and miR-1914-3p, as shown in Figure 3C, and the expression of MALAT1 and miR-1914-3p was negatively correlated in 31 peritraumatic tissues.

A targeting relationship between MALAT1 and miR-1914-3p was predicted based on the ENCORI, DIANA-LncBase and RNA22 databases (Figure 3D and E). We performed luciferase reporter gene, RIP and RNA pull-down assays to verify the above speculation further. The luciferase reporter gene experiments showed that miR-1914-3p mimic significantly reduced the relative luciferase activity of MALAT1-WT. At the same time, no similar effect was observed on the luciferase activity of MALAT1-MUT compared to mimic-NC treatment (Figure 3F). To further explore the occurrence of the RNA-induced silencing complex upon MALAT1 binding to miR-1914-3p, we performed a RIP assay. The results showed that the AGO2 antibody significantly enriched MALAT1 and miR-1914-3p, implying that MALAT1 could target miR-1914-3p by binding to AGO2 (Figure 3G). To further validate the direct binding of MALAT1 to miR-1914-3p, we combined bio-miR-1914- 3p-WT, bio-miR-1914-3p-MUT, bio-NC respectively, after transfection into HEK 293T cells for RNA pull-down. The results showed that Bio-miR-1914-3p-WT could pull down MALAT1, but Bio-miR-1914-3p-MUT had no significant effect on MALAT1 (Figure 3H), indicating a direct interaction between miR-1914-3p and MALAT1.

To verify whether MALAT1 could competitively bind to miR-1914-3p and regulate MFGE8 expression, we delivered plasmids, si-RNA and mimic into THP-1-derived macrophages to determine the expression of miR-1914-3p and MFGE8, respectively. RT-qPCR and WB results showed that MALAT1 overexpression resulted in miR-1914-3p expression. The results of RT-qPCR and WB showed that MALAT1 overexpression led to decreased miR-1914-3p expression and increased MFGE8 expression, while si-MALAT1 treatment induced increased miR-1914-3p expression and decreased MFGE8 expression, while oe-MALAT1 and miR-1914-3p mimic co-transfected THP-1-derived macrophages showed no significant changes in miR-1914-3p and MFGE8 expression, indicating that MALAT1 was able to competitively bound to miR-1914-3p and regulate MFGE8 expression competitively (Figure 3I, O and P). The subsequent changes in macrophage phagocytosis (Figure 3J, K and Supplementary Figure 3B), apoptosis (Figure 3L and M) and polarization (Figure 3N-P) were verified by flow, RT-qPCR and WB. RT-qPCR and WB determined the expression of TGFB1 and SMAD3(Figure 3N-P). The results showed that transduction of oe-MALAT1 promoted macrophage phagocytosis, inhibited apoptosis, and promoted the conversion of macrophages to the M2 type, and TGFB1 and SMAD3 expression was significantly reduced. In contrast, the opposite was true for the si-MFGE8 treatment. It can be reasonably concluded that MALAT1 promoted macrophage phagocytosis, inhibited apoptosis, promoted macrophage polarize toward the M2 type, and inhibited TGFB1/SMAD3 signaling pathway activity through down-regulation of miR-1914-3p.

Characterization KCs-Derived Exosomes

A previous study has reported that KCs can promote the diabetic wound healing process.[35] Hereby, we examined the characteristics of exosomes in vitro to explore the function of exosomes from KCs in the diabetic wound-healing process. We first cultured keratinocytes, then transfected them with oe-MATAL1, oe-NC, si-MATAL1 or si-NC, collected their supernatants, and isolated exosomes. Pure exosomes produced were examined by Western blot, nanoparticle tracking analysis (NTA), and transmission electron microscopy (TEM). Transmission electron microscopy found that these particles are cup-shaped or spherical, which is consistent with past investigations (Figure 4A). Comparable to past research on exosome size, NTA found particles with a size range of 30 to 200 nanometers (Figure 4B). Exosome-specific surface markers, including CD63 and TSG101, were present on these particles, and Western blot later confirmed this (Figure 4C). The results indicate that the separated nanoparticles are exosomes.

KCs Regulated Expression of miR-1914-3p and MFGE8 in Macrophage by KCs-Exo Carrying MALAT1

To demonstrate that macrophages were indeed able to take up exosomes derived from KCs, DiI-labelled exosomes (red) were cultured together with THP-1-derived macrophages. The uptake of exosomes was observed under confocal fluorescence microscopy at the 6th, 12nd and 24th hour after incubation (Figure 5A). The results showed that the uptake

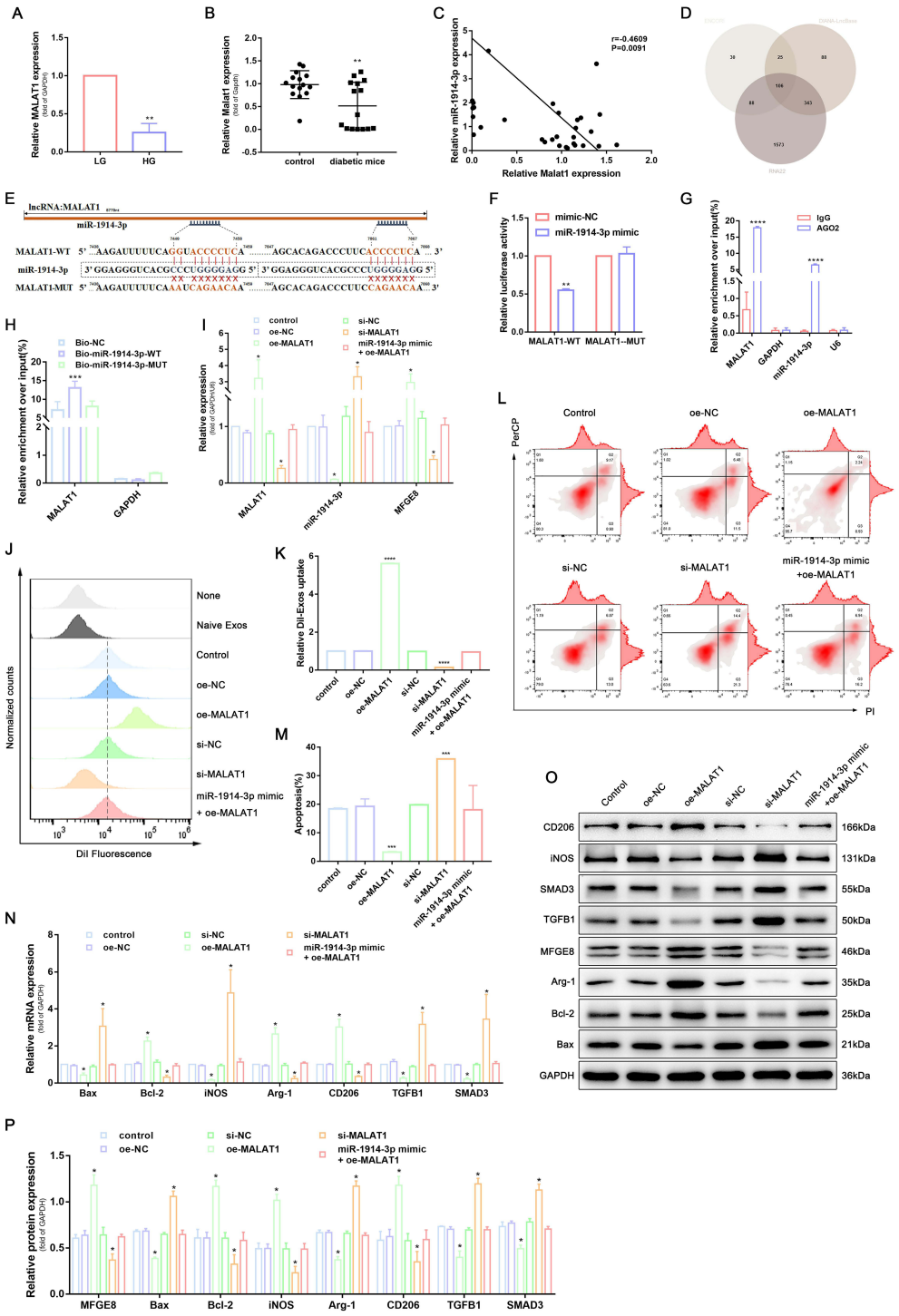

Figure 3 MALAT1 competitively bound to miR-1914-3p to inhibit the activity of the TGFB1/SMAD3 signaling pathway and affect macrophage phagocytosis, apoptosis, and polarization. (**A**) MALAT1 expression in a normal medium or high glucose medium, determined by qRT-PCR. (**B**) MALAT1 expression in wound tissue from normal mice or diabetic mice, determined by qRT-PCR. (**C**) The correlation between MALAT1 and miR-1914-3p expression, measured in 31 mice skin by Spearman correlation analysis. (**D**) Predicted target miRNAs of MALAT1 by three online databases (ENCORI, DIANA-LncBase and RNA22). (**E**) Predicted binding sites between MALAT1 and miR-1914-3p by bioinformatics database. (**F**) Luciferase activity of MALAT1-WT and MALAT1-MUT detected by dual-luciferase reporter gene assay. (**G**) Relative enrichment of Ago2 by MALAT1 and miR-1914-3p detected by RIP assay. (**H**) Relative enrichment of MALAT1 detected by RNA pull-down. (**I**) MALAT1, miR-1914-3p and mRNA expression of MFGE8 expression, determined by qRT-PCR. (**J** and **K**) Uptake of DiI-labelled KCs-Exo by PMA-treated THP-1 cells, measured by flow cytometry analysis. (**L** and **M**) Apoptosis in PMA-treated THP-1 cells, measured by flow cytometry analysis. (**N**) mRNA expression of apoptosis-related factors (Bax and Bcl-2), macrophage polarization-related surface markers (iNOS, Arg-1 and CD206), TGFB1 and SMAD3, determined by qRT-PCR. (**O** and **P**) Protein expression of apoptosis-related factors (Bax and Bcl-2), macrophage polarization-related surface markers (iNOS, Arg-1 and CD206), MFGE8, TGFB1 and SMAD3, normalized to GAPDH, determined by Western blot analysis. *p < 0.05, **p < 0.01, ***p < 0.001, ****p < 0.0001 versus the control group. Measurement data were expressed as mean ± SD. Comparison between two groups was conducted using independent sample *t* test. One-way ANOVA was used for data comparison among multiple groups, followed by Tukey's post hoc test. The experiment was repeated independently three times.

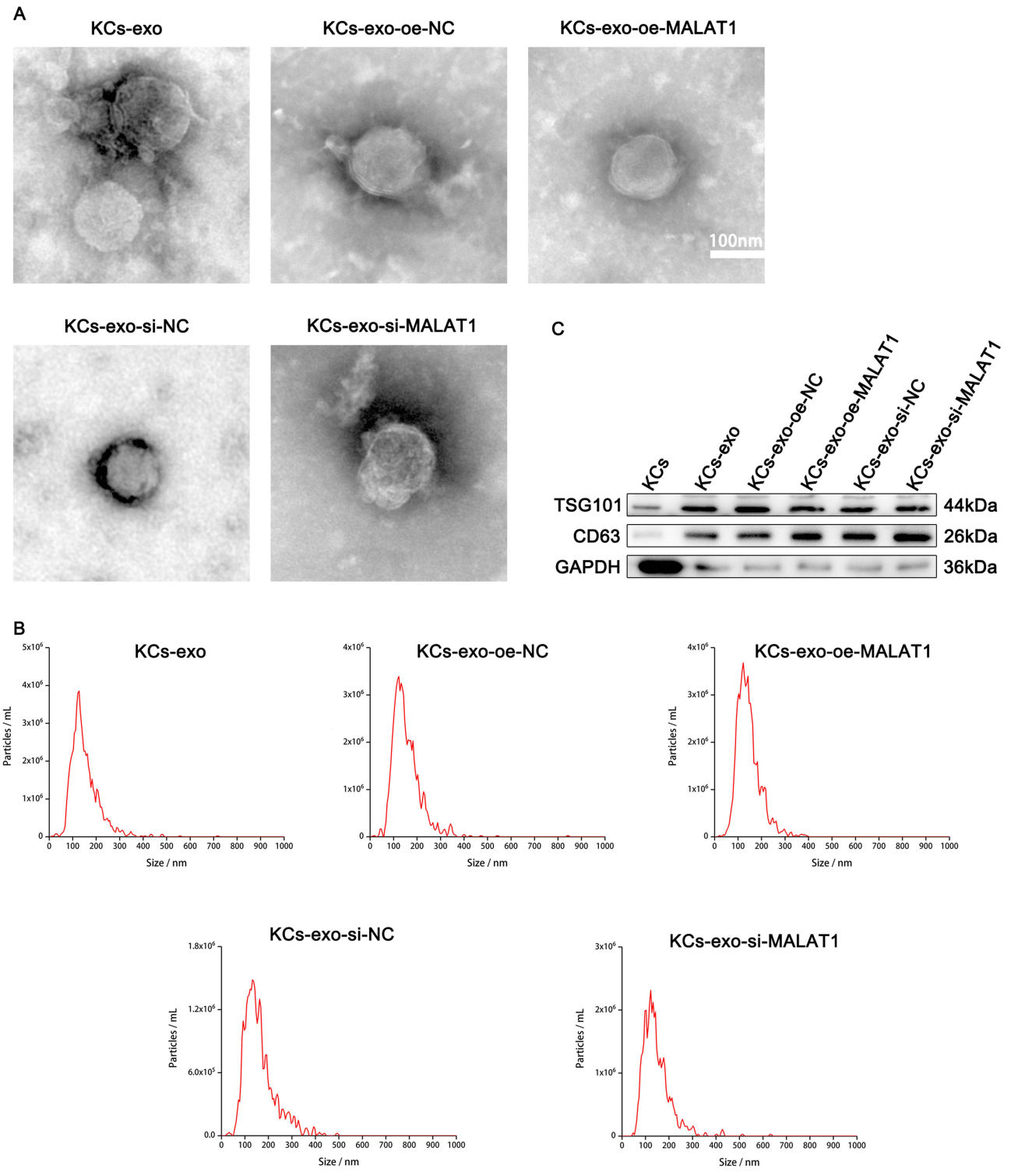

Figure 4 Characterization KCs-derived exosomes. (**A**) Morphology of exosomes observed by transmission electron microscopy; Scale bar: 100nm. (**B**) Particle size distribution of exosomes measured by NTA. (**C**) Exosome surface markers CD63 and TSG101 analysed by Western blot.

of DiI exosomes by THP-1-derived macrophages increased synchronously with increasing time. The uptake of exosomes was very evident after 24 h of co-culture, indicating that exosomes can be transferred from donor cells (KCs) to recipient cells (THP-1-derived macrophages). To confirm whether MALAT1 can be transferred to macrophages via KCs-exos, we altered the expression of MALAT1 in KCs using siRNA and plasmids and quantified MALAT1 in KCs and KCs-exos

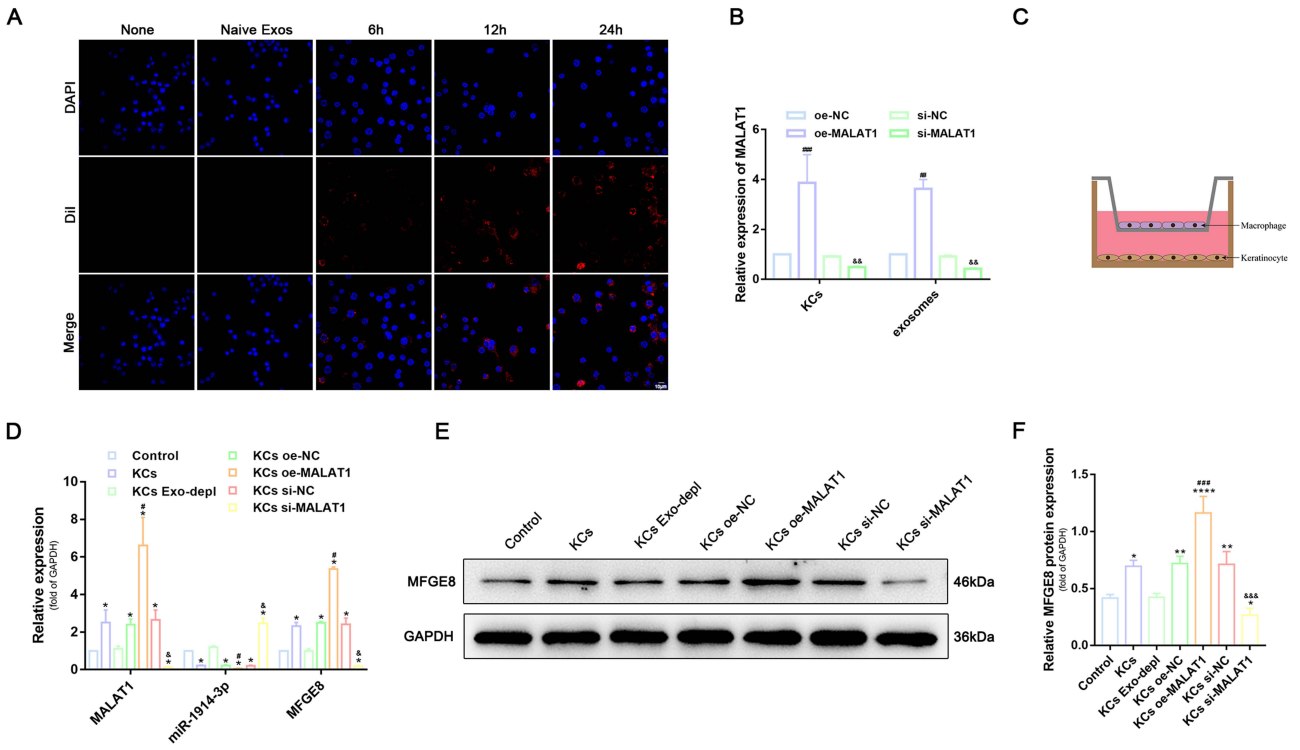

Figure 5 KCs regulated expression of miR-1914-3p and MFGE8 in macrophage by KCs-Exo carrying MALAT1. (**A**) The uptake of KCs-exo by PMA-treated THP-1 cells observed under an inverted microscope (600x), blue flurescence represents nucleus, red flurescence represents exosomes, Scale bar:10μm. (**B**) Expression of MALAT1 in KCs and exosomes, determined by qRT-PCR. (**C**) Schematic diagram of PMA-treated THP-1 cells and HaCaT co-culture system. (**D**) MALAT1 and miR-1914-3p expression, and mRNA expression of MFGE8, determined by qRT-PCR. (**E** and **F**) Protein expression of MFGE8, normalized to GAPDH determined by Western blot analysis. *p < 0.05, **p < 0.01, ****p < 0.0001 versus the control group (PMA-treated THP-1 cells without any treatment); #p < 0.05, ### p < 0.001 versus the oe-NC group (KCs treated with oe-NC); andp < 0.05, andandand p < 0.001 versus the si-NC group (KCs treated with si-NC). Measurement data were expressed as mean ± SD. One-way ANOVA was used for data comparison among multiple groups, followed by Tukey's post hoc test. The experiment was repeated independently three times.

using RT-qPCR. The results showed that MALAT1 expression was increased in KCs and KCs-exos in the presence of oe-MALAT1, whereas MALAT1 expression was decreased in the presence of si-MALAT1 (Figure 5B). To further confirm whether the transfer of MALAT1 could regulate the expression of miR-1914-3p and MFGE8 in macrophages, we used a co-culture system in which groups of KCs were plated on the 6-well basolateral chambers. In contrast, apical compartments were added with THP-1-derived macrophages (Figure 5C). RT-qPCR and Western blot analysis were used to quantify the expression of MALAT1, miR-1914-3p and MFGE8 in macrophages (Figure 5D-F). Compared to macrophages without any treatment, the expression of MALAT1, miR-1914-3p and MFGE8 were not significantly different when the secretion of KCs exosomes was blocked by GW4869. oe-MALAT1 treatment of KCs resulted in a significant decrease in miR-1914-3p expression and a substantial increase in MALAT1 and MFGE8 expression when the si-MALAT1 group was the exact opposite. This indicates that in vitro transfer of MALAT1 can effectively down-regulate miR-1914-3p expression and up-regulate MFGE8 expression. The above results clarify that the transfer of exogenous MALAT1 from KCs to macrophages is exosome-dependent.

KCs-Exo Carrying MALAT1 Regulated Macrophage Phagocytosis, Apoptosis, and Polarization via the TGFB1/SMAD3 Signaling Pathway

Since KCs can carry MALAT1 into macrophages via exosomes, we investigated the regulatory effects of exosomes on macrophage phagocytosis, apoptosis and polarization by co-culturing KCs-Exos with THP-1-derived macrophages. KCs-oe-MALAT1-Exos promoted THP-1-derived macrophages phagocytosis (Figure 6A, B and Supplementary Figure 3C) and inhibited apoptosis (Figure 6C and D), while RT-qPCR and WB confirmed that Bcl-2 expression was increased and Bax expression was downregulated (Figure 6E-G). Meanwhile, KCs-oe-MALAT1-Exos also reduced the expression of M1 macrophage marker iNOS and increased the expression of M2 macrophage markers Arg-1 and CD206, while si-

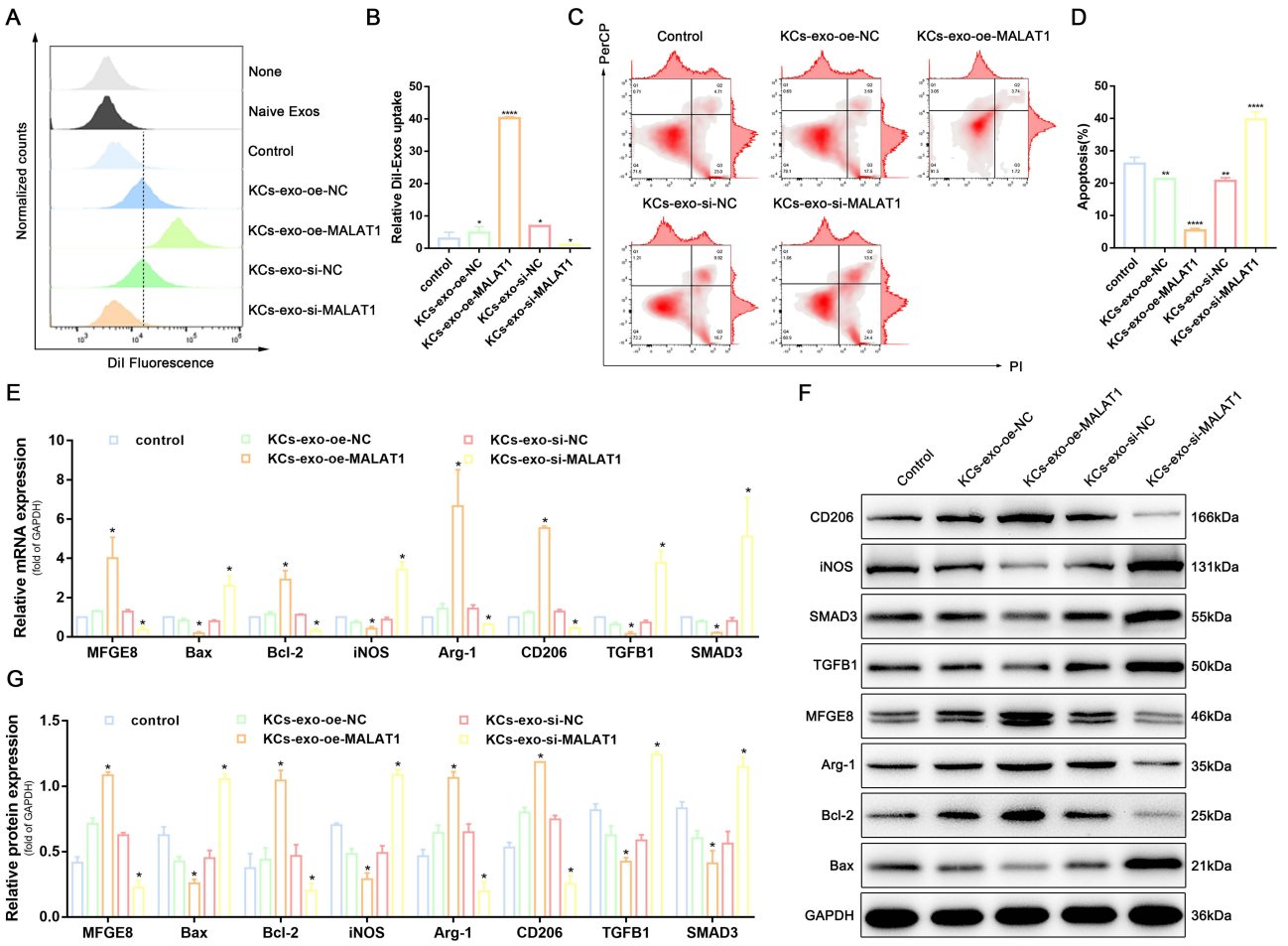

Figure 6 KCs-Exo carrying MALAT1 regulated macrophage phagocytosis, apoptosis, and polarization via the TGFB1/SMAD3 signaling pathway. (**A** and **B**) Uptake of DiI-labelled KCs-Exo by PMA-treated THP-1 cells, measured by flow cytometry analysis. (**C** and **D**) Apoptosis in PMA-treated THP-1 cells, measured by flow cytometry analysis. (**E**) mRNA expression of apoptosis-related factors (BAX and Bcl-2), macrophage polarization-related surface markers (iNOS, Arg-1 and CD206), MFGE8, TGFB1 and SMAD3, determined by qRT-PCR. (**F** and **G**) Protein expression of apoptosis-related factors (BAX and Bcl-2), macrophage polarization-related surface markers (iNOS, Arg-1 and CD206), MFGE8, TGFB1 and SMAD3, normalized to GAPDH, determined by Western blot analysis. *p < 0.05, **p < 0.01, ****p < 0.0001 versus the control group. Measurement data were expressed as mean ± SD. Comparison between two groups was conducted using independent sample *t* test. One-way ANOVA was used for data comparison among multiple groups, followed by Tukey's post hoc test. The experiment was repeated independently three times.

MALAT1 did the opposite (Figure 6E-G). It is suggested that KCs-Exo carrying MALAT1 regulates macrophage phagocytosis, apoptosis, and polarization.

In this study, we propose that the effect of the MALAT1/miR-1914-3p/MFGE8 axis on macrophage biological functions may be achieved through the TGFB1/SMAD3 signaling pathway. RT-qPCR and WB were performed to determine the expression of TGFB1 and SMAD3. The results showed that MFGE8 expression was significantly increased, and TGFB1 and SMAD3 expression was significantly decreased in the KCs-oe-MALAT1-Exo group, while the opposite was true for the si-MALAT1 treatment (Figure 6E-G). It can be concluded that MALAT1 can alter the expression of TGFB1 and SMAD3. These findings reaffirm that the TGFB1/SMAD3 signaling pathway regulates the MALAT1/miR-1914-3p/MFGE8 axis in macrophage phagocytosis, apoptosis and polarization.

KCs -Exo Carrying MALAT1 Promoted Wound Healing in Mice with Diabetes Mellitus

We created a type 2 diabetic mouse model and injected KCs-oe-MALAT1-exos into tissues surrounding the wound to evaluate the effect of KCs-exos on the diabetic wound-healing process in vivo. Wound area, H&E staining, Masson's trichrome staining, and immunohistochemical staining were then performed to observe wound healing. The outcomes revealed that the tissues injected with KCs-oe-MALAT1-exos healed more quickly, had more appropriate re-

epithelialization and granulation tissue, and less inflammatory cell infiltration than the diabetes group (Figure 7A-C). As the wound was examined under a microscope, it became clear that MALAT1 considerably sped up wound healing compared to the diabetic group (Figure 7C). Masson trichrome staining revealed more collagen deposition in the KCs-oe-MALAT1-exos group, demonstrating MALAT1's full capacity to remodel the ECM (Figure 7D). Finally, immunohistochemical testing of VEGF and CD31 was done to confirm the wound's vascular remodeling. The findings suggested that KCs-Exo expressing oe-MALAT1 might stimulate wound angiogenesis and consequently wound healing in mice by increasing VEGF and CD31(Figure 7E and F). Then, we used Western blot analysis to find the expression of MFGE8, TGFB1, and SMAD3 for further confirmation. Injection of KCs-oe-MALAT1-exos significantly reduced the expression of TGFB1, and SMAD3 while increasing the expression of MFGE8 (Figure 7G and H). This finding further supports the theory that MALAT1 speeds up wound healing by inhibiting the TGFB1/SMAD3 axis via binding to miR-1914-3p/MFGE8 in vivo. In conclusion, it was proposed that KCs-exos containing overexpressed MALAT1 might quicken diabetic mice's wound healing.

Discussion

Diabetes mellitus (DM) is a metabolic disease with a wide range of comorbidities that poses a significant threat to human health worldwide.[36] At the same time, it is well known that the delayed healing of diabetic complications is a huge threat to the health and even the lives of patients.[1] Various cells in the wound area will interact with each other through the secretion of cytokines to improve cellular function and advance the dynamic process of wound healing.[37] KCs, as the main component cells of the skin epidermis, play an important role in skin repair after damage.[35] It has been reported that inhibition of KCs biological functions will inhibit the wound healing process.[38,39] In addition to the direct involvement in the wound repair process through re-epithelialization and closure of the wound, the mechanism by which KCs exchange information with other skin cells such as macrophages[15] and epithelial cells[40] through secreted exosomes, thus promoting wound repair, has also been reported as one of the important mechanisms involved in the regulation of wound healing. Exosomes are membranous vesicles containing a variety of biologically active molecules that dock with other cells to accomplish intercellular communication and functional regulation.[41] As a paracellular secretory biocarrier, it has great research potential in healing and regenerating wounds.[42] Interestingly, various nucleic acids, including lncRNAs, have been identified in exosomes.[43] MALAT1, a lncRNA, maybe a transcriptional regulator of many genes, including some involved in cancer metastasis, cell migration and cell cycle regulation.[44,45] It is overexpressed in various cancer tissues, which is associated with tumour cell proliferation and metastasis.[6,46] Reducing MALAT1 expression would inhibit the reduction of vascular ingrowth in vivo, promoting atherosclerosis and plaque inflammation.[47] This study aimed to investigate the role of exosomes of keratinocyte HaCaT-derived high expression of MALAT1 in diabetic wound healing. We verified the low expression of MALAT1 in diabetic skin trauma tissue and in macrophages exposed to high glucose by RT-qPCR. In addition, RT-qPCR also demonstrated high MALAT1 expression in KCs-oe-MALAT1-exos. By injecting different groups of KCs-derived exosomes into the wound edges, we found that wound healing was significantly faster after KCs-oe-MALAT1-exos treatment and was complete after 21 days. H&E, Masson's staining and IHC further confirmed these observations. We confirmed that MALAT1 expressed in KCs-exosomes is a key candidate molecule for regulating the wound healing. Macrophages are the key to timely wound healing.[48] Our study found that the removal of macrophages from mice resulted in significantly slower wound healing, poorer tissue healing and a significant reduction in collagen. The IHC further confirms these observations.

Normal wound healing can be roughly divided into 3 phases: hemostatic inflammatory, proliferative, and remodeling phase.[37] Macrophages are predominantly classically activated (M1) during the inflammatory phase and are involved in cell destruction and phagocytosis of microorganisms, apoptosis and necrotic tissue. Subsequently, macrophages transform into alternatively activated (M2) cells, which drive wound healing into the proliferative phase.[49] Diabetic trauma usually shows persistent polarization of M1-type macrophages.[50,51] A study demonstrated that subcutaneous injection of M2 macrophage exosomes into mouse wounds promoted the conversion of M1 macrophages to M2 in wounds, thereby promoting wound healing.[52] Primary macrophages have limited proliferation capacity in vitro, while PMA-treated THP-1 cells retain macrophage polarization, phagocytosis, and secretion functions and are readily available. Therefore, PMA-treated THP-1 cells are often considered a macrophage equivalent for mimicking macrophage functions.[53] The present

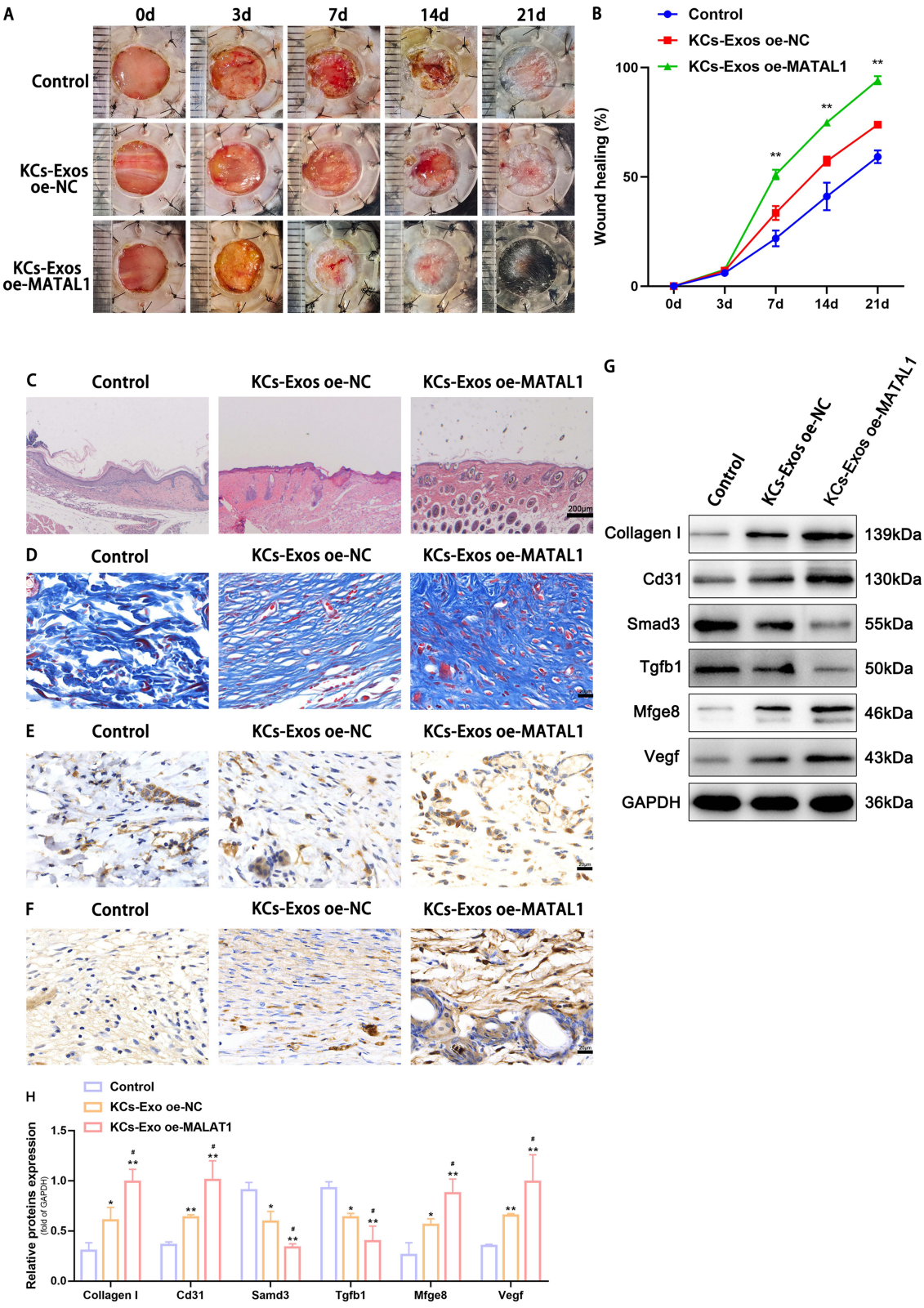

Figure 7 KCs -Exo carrying MALAT1 promoted wound healing in mice with diabetes mellitus. (**A**) Representative images of full thickness defects in mice at days 0, 3, 7, 14, and 21 days postoperatively. (**B**) Wound healing closure rates was calculated among the different groups using the ImageJ software. (**C**) H&E staining among the different groups at day 14, Scale bar: 200μm. (**D**) Masson's trichrome staining among the different groups at day 14, Scale bar: 20μm. (**E**) Representative immunohistochemical images of CD31, Scale bar: 20μm. (**F**) Representative immunohistochemical images of VEGF, Scale bar: 20μm. (**G** and **H**) Relative protein expression of Collagen I, Cd31, Smad3, Tgfb1, Mfge8, Vegf determined by Western blot analysis. *p < 0.05, **p < 0.01 versus the control group; #p < 0.05 versus the KCs-Exo oe-NC group. Measurement data were expressed as mean ± SD. Comparison among multiple groups was conducted using one-way ANOVA, followed by Tukey's post hoc test.

study also used PMA to induce differentiation of the human monocytes to macrophages. It was shown that the phagocytosis of apoptotic cells[54] and nanoparticlesby[55] PMA-treated THP-1 cells was significantly higher after polarization toward M2.

Low expression of phagocytosis-related molecules was found in peroxisome proliferator-activated receptor γ (PPARγ) knockout cells, and apoptotic cell accumulation and slowed wound healing were found in PPARγ-KO murine wounds.[56] In addition, activation of phagocytosis-related pathways converts macrophages to a prohealing phenotype(M2).[12] Meanwhile, phagocytosis of apoptotic neutrophils is essential for transforming the macrophage phenotype to an anti-inflammatory phenotype(M2).[57] In summary, the phagocytosis of macrophages and their phenotypic conversion complement each other and promote each other in the process of wound healing. Furthermore, a previous publication reported that exosomes from MSCs treated with LPS highly expressed let-7b, promoting wound healing by activating M2-type macrophages and down-regulating inflammatory factor.[58] A study also used tissue nano-transfection (TNT) to label KCs-Exos, thus demonstrating that KCs-Exos would be selectively phagocytosed by macrophages in wound granulation tissue.[15] Therefore, we hypothesized that MALAT1 in KCs-Exos could regulate macrophage biological functions. M1 macrophages have been reported to express pro-inflammatory cytokines and induced nitric oxide synthase, while M2 macrophages express arginase 1, mannose receptor CD206 and IL-4 receptor alpha chain.[49] These indicators can also identify the polarization status of THP-1-derived macrophages.[59,60] Therefore, we chose iNOS, Arg-1 and CD206 as indicators to detect macrophage polarization. Meanwhile, since BAX and Bcl2 are key factors in the process of apoptosis,[61] the correlation and ratio of the two determine the survival or death of cells after apoptotic stimulation.[62] Most of the studies have used the examination of BAX and BCL2 expression levels to verify apoptosis.[61–64] Therefore, we likewise chose BAX and Bcl-2 as indicators to detect apoptosis. We found that human monocyte-derived macrophages co-cultured with KCs-oe-MALAT1-Exo possessed greater cytophagocytosis, weaker apoptosis and a greater tendency to polarize towards the M2 phenotype. These findings suggest that direct transplantation of KCs-oe-MALAT1-Exo may promote wound healing by modulating macrophage bioactivity.

Sustained polarization of M1-type macrophages leads to a prolonged inflammatory response and persistent oxidative stress.[65] Another major reason for the failure of diabetic wounds to heal is redox imbalance due to excessive oxidative stress and decreased antioxidant capacity.[66] The combination of azilsartan and NF-kB inhibitor (Bay11-7082) has been reported to promote apoptosis in hepatocellular carcinoma cells by increasing reactive oxygen species (ROS) production and upregulating oxidation levels.[64] It has also been confirmed that nano-antioxidants have a significant effect on improving oxidative stress levels.[63] Poor oxygen perfusion and impaired skin barrier due to oxidative stress and circulatory dysfunction will also increase the susceptibility of diabetic trauma infections.[66] A silver nanoparticle modified by urea based periodic mesoporous organosilica (AgNPs/Ur-PMO) was shown to have excellent antibacterial effect in in vitro experiments.[67] Another exosome (PCOF@E-Exo) encapsulated by cationic antimicrobial carbon dots (CDs) derived from hypoxic conditioned TNF-α treated mesenchymal stem cells was validated by in vivo experiments to have beneficial effects in inhibiting oxidative damage, tissue inflammation and clearing bacterial infections.[68] What we do know is that mitochondria are a key site for the onset of oxidative stress and can be a possible therapeutic target.[69] Therefore, nanoparticles targeting mitochondria and carrying antioxidant drugs may be able to exert drug effects more efficiently. An in vivo study confirmed that MSC-derived extracellular vesicles (MSC- Evs) can increase mitochondrial transcription factor A (TFAM) and mitochondrial DNA (mtDNA) levels, thereby reducing kidney injury, mitochondrial damage and inflammation in mice with acute kidney injury.[70] Our study confirmed that KCs-oe-MALAT1-Exo promotes macrophage polarization toward M2 type. Taken together, to some extent, we speculate that this exosome may also have anti-inflammatory and antioxidant effects by repairing mtDNA. We provide evidence for the potential clinical application of KCs-Exo in wound healing. With these encouraging results from ex vivo studies, we further reveal possible mechanisms by which MALAT1 regulates wound healing. There is growing evidence for ceRNA as a mechanism to regulate wound healing. For example, LncRNA GAS5 up-regulates Prox1 to promote lymphangiogenesis and diabetic wound healing by spongy acting on miR-217.[71] LncRNA XIXT promotes the proliferation and migration of fibroblasts and the polarization of M2 macrophages by targeting miR-19b.[72] As a lncRNA, MALAT1 can also exert its biological functions, such as binding to miR-124[7] or miR-378a[8] to promote wound healing, miR-142-3p[9] to accelerate endometrial stromal cell proliferation and inhibit cell apoptosis. Our study revealed a negative correlation between the high

expression of miR-1914-3p and the low expression of MALAT1 in the skin tissues of diabetic mice. In addition, the miR-1914-3p mimic reversed the downregulation of miR-1914-3p expression caused by oe-MALAT1, inhibited macrophage phagocytosis and polarization to M2 type, and promoted macrophage apoptosis. Furthermore, both databases and experiments have verified that MALAT1 binds to miR-1914-3p, which has also been reported in the literature and induces drug resistance and metastasis in NSCLC.[6] These findings suggest that MALAT1 competitively binds to miR-1914-3p to form ceRNAs that regulate macrophage biological functions and drive the wound healing process.

In addition, MFGE8, a protein also differentially expressed in the diabetic wound, was predicted by bioinformatics to contain the target site of miR-1914-3p in its 3'UTR. It has been reported that MFGE8 is a secretory glycoprotein ubiquitously expressed in various organs and cells that can interact with macrophages, which can be combined with αvβ3-integrin and phosphorylated serine sites, respectively.[73] MFGE8 can reduce inflammation,[11,14] activate phagocytic signals,[12] induce polarization of M2-type macrophages,[13,74] promote angiogenesis,[34] and improve fibroblast migration.[74] It has been found that long-term hyperglycemia and advanced glycation end products deactivate MFGE8 in diabetic tissues, which is an important mechanism for the difficult healing of diabetic wounds.[34] Similarly, in the present study, we found that MFGE8 was negatively correlated with miR-1914-3p. Dual luciferase assay further confirmed the direct binding of miR-1914-3p to MFGE8 3'UTR. In addition, the upregulation of MFGE8 expression induced by oe-MALAT1 was inhibited by miR-1914-3p mimic. oe-MFGE8 could reverse the reduction of MFGE8 expression induced by miR-1914-3p mimic, promote phagocytosis and M2 polarization of macrophages, and inhibit apoptosis of macrophages. These data suggest that MALAT1 in Exos regulates skin wound healing by binding to miR-1914-3p to up-regulate MFGE8 expression.

Multiple studies have shown that MFGE8 is a negative regulator upstream of TGFB1/SMAD3.[75,76] Therefore, we examined whether MALAT1 in KCs-Exo would similarly alter TGFB1 and SMAD3 in macrophages. RT-qPCR and WB verified that oe-MALAT1, miR-1914-3p mimic, and oe-MFGE8 significantly inhibited TGFB1 and SMAD3 mRNA and protein levels. Combined with the results of our in vivo experiments, it was revealed that the MALAT1 /miR-1914-3p/MFGE8 pathway could promote wound healing by suppressing TGFB1/SMAD3. Interestingly, TGFB1 and SMAD3, which are growth factors involved in multiple biological functions, showed a decreasing trend in our faster healing group. TGFB1 is widely expressed and plays biological roles in organisms. Numerous studies have shown that TGFB1 plays an important role in tissue fibrosis, wound contraction and scar formation, while high activation of the SMAD2/3 pathway is also pro-fibrotic.[77–80] Persistent activation of the TGFB/SMAD signaling pathway leads to prolonged overactivation of fibroblasts, extracellular matrix (ECM) deposition, and abnormal collagen accumulation.[78] Compared with normal adult skin, the expression of TGFB1 in early pregnancy fetal skin, which can heal without a scar, is significantly decreased.[81,82] The expression levels of SMAD2 and SMAD7 are significantly higher in hypertrophic scar fibroblasts (HSFs) than in normal skin fibroblasts (NSFs), and TGFB1 can further stimulate SMAD production.[83] In addition, it was confirmed that hBM-MSC-exos significantly down-regulated the expression of TGFB1 and SMAD3 while effectively promoting wound healing in the rat wound model.[84] Therefore, it is reasonable to conclude that the MALAT1 /miR-1914-3p/MFGE8 pathway can reduce scar formation in the process of promoting wound healing by down-regulating TGFB1/SMAD3.

High levels of oxidative stress have been demonstrated to be another major factor in delayed diabetic wound healing, and the application of nano-antioxidants and antimicrobial materials has been shown to be effective in promoting diabetic wound healing. Therefore, improving our existing exosomes to target the mitochondria of diabetic wound cells and deliver drugs or biomolecules to regulate the level of oxidative stress in wounds may be a new approach to promote diabetic wound healing. Meanwhile, further studies are needed regarding the temporal phasing of KCs-Exo MALAT1-initiated macrophage gene expression and the specific mechanism of MFGE8 interaction with the TGFB/SMAD3 pathway in KCs-Exo MALAT1 treatment. Subsequently, we will determine the mRNA expression profiles of traumatic tissues in each group of mice at different times. Then based on the analysis of bioinformatics methods, we will screen the differentially expressed genes and construct a protein-protein interaction (PPI) network to further investigate the mechanism of KCs-Exo MALAT1 in treating diabetic wound. We will also make an additional refinement of this exosome to discover more effective treatment options.

The results of this study both validate the findings of previous studies and explore possible mechanisms of delayed healing of diabetic wounds, as well as validate the feasibility of KCs-Exo MALAT1 for the treatment of diabetic wounds. In conclusion, our results demonstrate, for the first time in vitro and in vivo, that KCs-Exo high expression of MALAT1

improves macrophage function through disrupting miR-1914-3p-mediated MFGE8 inhibition and promotes the diabetic wound healing process, leading to better physiological and functional recovery of the wounds, which could provide a theoretical basis and therapeutic target for clinical treatment of diabetic wounds. The results of the study support further exploration of the exosomes generated by this protocol. This technique has relevance for future clinical applications and offers new possibilities for the treatment of diabetic wounds.

Conclusion

Our results revealed that human keratinocyte-derived exosomes facilitate skin wound repair via modulating the biologic capacity of macrophages in vitro and in vivo. By suppressing miR-1914-3p to activate MFGE8, the keratinocyte-derived exosomal MALAT1 promote wound healing by enhancing macrophage phagocytosis, converting to a pro-healing phenotype and reducing apoptosis. It will be fascinating to assess whether exosomes released by keratinocytes influence the wound repair response from other cell types. Based on our results, we think that in the future, nanomaterials combining with MALAT1 and MFGE8 might have the capacity to serve as a new method for the clinical treatment of diabetic wound.

Ethics Approval and Consent to Participate

All animal experiments confirmed to the Institutional Animal Care and Use Committee Tongji Medical College, Huazhong University of Science and Technology [2020 IACUC Number: 2729]. The Laboratory Animal Guidelines for Ethical Review of Animal Welfare (GB/T 35892-2018) was followed to ensure the welfare of the laboratory animals.

Acknowledgments

We would like to acknowledge Dr. Zhi Wang for providing suggestions.

Funding

This study was supported by the young Scientists Fund of the National Science Foundation of China (81801922), Hubei Science and Technology Department of chronic wounds and diabetic foot medical clinical research center construction project(2018BCC340), Hubei Province Key R &D Project(2020BCB029) and Natural Science Foundation of Hubei Province (2020CFB696).

Disclosure

All authors declare no conflicts of interest in this work.

References

1. Singh N, Armstrong DG, Lipsky BA. Preventing foot ulcers in patients with diabetes. *JAMA*. 2005;293(2):217–228.
2. Fu XL, Ding H, Miao WW, Mao CX, Zhan MQ, Chen HL. Global recurrence rates in diabetic foot ulcers: a systematic review and meta-analysis. *Diabetes Metab Res Rev*. 2019;35(6):e3160. doi:10.1002/dmrr.3160
3. Bakker K, Apelqvist J, Lipsky BA, Van Netten JJ. The 2015 IWGDF guidance documents on prevention and management of foot problems in diabetes: development of an evidence-based global consensus. *Diabetes Metab Res Rev*. 2016;32(Suppl 1):2–6. doi:10.1002/dmrr.2694
4. Everett E, Mathioudakis N. Update on management of diabetic foot ulcers. *Ann N Y Acad Sci*. 2018;1411(1):153–165. doi:10.1111/nyas.13569
5. Kuai L, Jiang J-S, Li W, Li B, Yin S-Y. Long non-coding RNAs in diabetic wound healing: current research and clinical relevance. *Int Wound J*. 2022;19(3):583–600. doi:10.1111/iwj.13655
6. Jin D, Guo J, Wu Y, et al. mA mRNA methylation initiated by METTL3 directly promotes YAP translation and increases YAP activity by regulating the MALAT1-miR-1914-3p-YAP axis to induce NSCLC drug resistance and metastasis. *J Hematol Oncol*. 2019;12(1):135. doi:10.1186/s13045-019-0830-6
7. He L, Zhu C, Jia J, et al. ADSC-Exos containing MALAT1 promotes wound healing by targeting miR-124 through activating Wnt/β-catenin pathway. *Bioscience Reports*. 2020;40(5). doi:10.1042/BSR20192549.
8. Pi L, Yang L, Fang B-R, Qian L. LncRNA MALAT1 from human adipose-derived stem cell exosomes accelerates wound healing via miR-378a/FGF2 axis. *Regen Med*. 2022;17(9). 627–641. doi:10.2217/rme-2021-0170
9. Tan K, Mo H, Guo L, Wang B. MALAT1 accelerates proliferation and inflammation and suppresses apoptosis of endometrial stromal cells via the microRNA-142-3p/CXCR7 axis. *Reprod Biol*. 2022;22(3):100675. doi:10.1016/j.repbio.2022.100675
10. Bushati N, Cohen SM. microRNA functions. *Annu Rev Cell Dev Biol*. 2007;23:175–205.
11. Huang W, Jiao J, Liu J, et al. MFG-E8 accelerates wound healing in diabetes by regulating "NLRP3 inflammasome-neutrophil extracellular traps" axis. *Cell Death Discovery*. 2020;6(1). doi:10.1038/s41420-020-00318-7.

12. Patil M, Saheera S, Dubey PK, et al. Novel Mechanisms of Exosome-Mediated Phagocytosis of Dead Cells in Injured Heart. *Circ Res*. 2021;129 (11):1006–1020. doi:10.1161/CIRCRESAHA.120.317900
13. Geng R, Lin Y, Ji M, et al. MFG-E8 promotes tendon-bone healing by regualting macrophage efferocytosis and M2 polarization after anterior cruciate ligament reconstruction. *J Orthop Translat*. 2022;34:11–21. doi:10.1016/j.jot.2022.04.002
14. Huang W, Wu J, Yang H, et al. Milk fat globule-EGF factor 8 suppresses the aberrant immune response of systemic lupus erythematosus-derived neutrophils and associated tissue damage. *Cell Death Differ*. 2017;24(2):263–275. doi:10.1038/cdd.2016.115
15. Zhou X, Brown BA, Siegel AP, et al. Exosome-Mediated Crosstalk between Keratinocytes and Macrophages in Cutaneous Wound Healing. *ACS Nano*. 2020;14(10):12732–12748. doi:10.1021/acsnano.0c03064
16. Li B, Luan S, Chen J, et al. The MSC-Derived Exosomal lncRNA H19 Promotes Wound Healing in Diabetic Foot Ulcers by Upregulating PTEN via MicroRNA-152-3p. *Molecular Therapy*. 2020;19:814–826. doi:10.1016/j.omtn.2019.11.034
17. Yang D, Zhang W, Zhang H, et al. Progress, opportunity, and perspective on exosome isolation - efforts for efficient exosome-based theranostics. *Theranostics*. 2020;10(8):3684–3707. doi:10.7150/thno.41580
18. Liang Y, Duan L, Lu J, Xia J. Engineering exosomes for targeted drug delivery. *Theranostics*. 2021;11(7):3183–3195. doi:10.7150/thno.52570
19. Alvarez-Erviti L, Seow Y, Yin H, Betts C, Lakhal S, Wood MJA. Delivery of siRNA to the mouse brain by systemic injection of targeted exosomes. *Nat Biotechnol*. 2011;29(4):341–345. doi:10.1038/nbt.1807
20. Wang B, Zhang A, Wang H, et al. miR-26a Limits Muscle Wasting and Cardiac Fibrosis through Exosome-Mediated microRNA Transfer in Chronic Kidney Disease. *Theranostics*. 2019;9(7):1864–1877. doi:10.7150/thno.29579
21. Bader JE, Enos RT, Velázquez KT, et al. Macrophage depletion using clodronate liposomes decreases tumorigenesis and alters gut microbiota in the AOM/DSS mouse model of colon cancer. *Am J Physiol Gastrointest Liver Physiol*. 2018;314(1):G22–G31. doi:10.1152/ajpgi.00229.2017
22. Lin H-N, O'Connor JP. Osteoclast depletion with clodronate liposomes delays fracture healing in mice. *J Orthop Res*. 2017;35(8):1699–1706. doi:10.1002/jor.23440
23. Xiong Y, Chen L, Yan C, et al. Circulating Exosomal miR-20b-5p Inhibition Restores Wnt9b Signaling and Reverses Diabetes-Associated Impaired Wound Healing. *Small*. 2020;16(3):e1904044. doi:10.1002/smll.201904044
24. Li B, Luan S, Chen J, et al. The MSC-Derived Exosomal lncRNA H19 Promotes Wound Healing in Diabetic Foot Ulcers by Upregulating PTEN via MicroRNA-152-3p. *Mol Ther Nucleic Acids*. 2020;19:814–826.
25. Liu W, Yu M, Xie D, et al. Melatonin-stimulated MSC-derived exosomes improve diabetic wound healing through regulating macrophage M1 and M2 polarization by targeting the PTEN/AKT pathway. *Stem Cell Res Ther*. 2020;11(1):259. doi:10.1186/s13287-020-01756-x
26. Yu M, Liu W, Li J, et al. Exosomes derived from atorvastatin-pretreated MSC accelerate diabetic wound repair by enhancing angiogenesis via AKT/eNOS pathway. *Stem Cell Res Ther*. 2020;11(1):350. doi:10.1186/s13287-020-01824-2
27. Ren S, Chen J, Guo J, et al. Exosomes from Adipose Stem Cells Promote Diabetic Wound Healing through the eHSP90/LRP1/AKT Axis. *Cells*. 2022;11:20. doi:10.3390/cells11203229
28. Sticht C, De La Torre C, Parveen A, Gretz N. miRWalk: an online resource for prediction of microRNA binding sites. *PLoS One*. 2018;13(10): e0206239. doi:10.1371/journal.pone.0206239
29. Li J-H, Liu S, Zhou H, Qu L-H, Yang J-H. starBase v2.0: decoding miRNA-ceRNA, miRNA-ncRNA and protein-RNA interaction networks from large-scale CLIP-Seq data. *Nucleic Acids Res*. 2014;42:D92–D97. doi:10.1093/nar/gkt1248
30. McGeary SE, Lin KS, Shi CY, et al. The biochemical basis of microRNA targeting efficacy. *Science*. 2019;366:6472. doi:10.1126/science.aav1741
31. Miranda KC, Huynh T, Tay Y, et al. A pattern-based method for the identification of MicroRNA binding sites and their corresponding heteroduplexes. *Cell*. 2006;126(6):1203–1217. doi:10.1016/j.cell.2006.07.031
32. Karagkouni D, Paraskevopoulou MD, Tastsoglou S, et al. DIANA-LncBase v3: indexing experimentally supported miRNA targets on non-coding transcripts. *Nucleic Acids Res*. 2020;48(D1):D101–D110. doi:10.1093/nar/gkz1036
33. Li X, Li N, Li B, Feng Y, Zhou D, Chen G. Noncoding RNAs and RNA-binding proteins in diabetic wound healing. *Bioorg Med Chem Lett*. 2021;50:128311. doi:10.1016/j.bmcl.2021.128311
34. Das A, Ghatak S, Sinha M, et al. Correction of MFG-E8 Resolves Inflammation and Promotes Cutaneous Wound Healing in Diabetes. *J Immunol*. 2016;196(12):5089–5100.
35. Blanpain C, Fuchs E. Epidermal stem cells of the skin. *Annu Rev Cell Dev Biol*. 2006;22:339–373. doi:10.1146/annurev.cellbio.22.010305.104357
36. Sun H, Saeedi P, Karuranga S, et al. IDF Diabetes Atlas: global, regional and country-level diabetes prevalence estimates for 2021 and projections for 2045. *Diabetes Res Clin Pract*. 2022;183:109119. doi:10.1016/j.diabres.2021.109119
37. Wang P-H, Huang B-S, Horng H-C, Yeh -C-C, Chen Y-J. Wound healing. *J Chin Med Assoc*. 2018;81(2). doi:10.1016/j.jcma.2017.11.002
38. Qu H, Miao T, Wang Y, et al. Dedicator of Cytokinesis 5 Regulates Keratinocyte Function and Promotes Diabetic Wound Healing. *Diabetes*. 2021;70(5):1170–1184. doi:10.2337/db20-1008
39. Yang DJ, Moh SH, Choi Y-H, Kim KW. β-Neoendorphin Enhances Wound Healing by Promoting Cell Migration in Keratinocyte. *Molecules*. 2020;25:20. doi:10.3390/molecules25204640
40. Leszczynska A, Kulkarni M, Ljubimov AV, Saghizadeh M. Exosomes from normal and diabetic human corneolimbal keratocytes differentially regulate migration, proliferation and marker expression of limbal epithelial cells. *Scientific Reports*. 2018;8(1):15173. doi:10.1038/s41598-018-33169-5
41. Jeppesen DK, Fenix AM, Franklin JL, et al. Reassessment of Exosome Composition. *Cell*. 2019;177(2):428–445.e18. doi:10.1016/j.cell.2019.02.029
42. Wu P, Zhang B, Shi H, Qian H, Xu W. MSC-exosome: a novel cell-free therapy for cutaneous regeneration. *Cytotherapy*. 2018;20(3):291–301. doi:10.1016/j.jcyt.2017.11.002
43. Sato-Kuwabara Y, Melo SA, Soares FA, Calin GA. The fusion of two worlds: non-coding RNAs and extracellular vesicles--diagnostic and therapeutic implications (Review). *Int J Oncol*. 2015;46(1):17–27. doi:10.3892/ijo.2014.2712
44. Mao T-L, Fan M-H, Dlamini N, Liu C-L. LncRNA MALAT1 Facilitates Ovarian Cancer Progression through Promoting Chemoresistance and Invasiveness in the Tumor Microenvironment. *International Journal of Molecular Sciences*. 2021;22:19. doi:10.3390/ijms221910201
45. Kim J, Piao H-L, Kim B-J, et al. Long noncoding RNA MALAT1 suppresses breast cancer metastasis. *Nat Genet*. 2018;50(12):1705–1715. doi:10.1038/s41588-018-0252-3
46. Jen J, Tang Y-A, Lu Y-H, Lin -C-C, Lai -W-W, Wang Y-C. Oct4 transcriptionally regulates the expression of long non-coding RNAs NEAT1 and MALAT1 to promote lung cancer progression. *Mol Cancer*. 2017;16(1):104. doi:10.1186/s12943-017-0674-z

47. Cremer S, Michalik KM, Fischer A, et al. Hematopoietic Deficiency of the Long Noncoding RNA MALAT1 Promotes Atherosclerosis and Plaque Inflammation. *Circulation*. 2019;139(10):1320–1334. doi:10.1161/CIRCULATIONAHA.117.029015
48. Sharifiaghdam M, Shaabani E, Faridi-Majidi R, De Smedt SC, Braeckmans K, Fraire JC. Macrophages as a therapeutic target to promote diabetic wound healing. *Mol Ther*. 2022;30(9):2891–2908. doi:10.1016/j.ymthe.2022.07.016
49. Murray PJ, Wynn TA. Protective and pathogenic functions of macrophage subsets. *Nat Rev Immunol*. 2011;11(11):723–737. doi:10.1038/nri3073
50. Louiselle AE, Niemiec SM, Zgheib C, Liechty KW. Macrophage polarization and diabetic wound healing. *Transl Res*. 2021;236:109–116. doi:10.1016/j.trsl.2021.05.006
51. Al Sadoun H. Macrophage Phenotypes in Normal and Diabetic Wound Healing and Therapeutic Interventions. *Cells*. 2022;11:15. doi:10.3390/cells11152430
52. Kim H, Wang SY, Kwak G, Yang Y, Kwon IC, Kim SH. Exosome-Guided Phenotypic Switch of M1 to M2 Macrophages for Cutaneous Wound Healing. *Adv Sci*. 2019;6(20):1900513. doi:10.1002/advs.201900513
53. Daigneault M, Preston JA, Marriott HM, Whyte MKB, Dockrell DH. The identification of markers of macrophage differentiation in PMA-stimulated THP-1 cells and monocyte-derived macrophages. *PLoS One*. 2010;5(1):e8668. doi:10.1371/journal.pone.0008668
54. Shiratori H, Feinweber C, Luckhardt S, et al. THP-1 and human peripheral blood mononuclear cell-derived macrophages differ in their capacity to polarize in vitro. *Mol Immunol*. 2017;88:58–68. doi:10.1016/j.molimm.2017.05.027
55. Hoppstädter J, Seif M, Dembek A, et al. M2 polarization enhances silica nanoparticle uptake by macrophages. *Front Pharmacol*. 2015;6:55. doi:10.3389/fphar.2015.00055
56. Chen H, Shi R, Luo B, et al. Macrophage peroxisome proliferator-activated receptor γ deficiency delays skin wound healing through impairing apoptotic cell clearance in mice. *Cell Death Dis*. 2015;6:e1597. doi:10.1038/cddis.2014.544
57. Sousa AB, Águas AP, Barbosa MA, Barbosa JN. Immunomodulatory biomaterial-based wound dressings advance the healing of chronic wounds via regulating macrophage behavior. *Regen Biomater*. 2022;9:rbac065. doi:10.1093/rb/rbac065
58. Ti D, Hao H, Tong C, et al. LPS-preconditioned mesenchymal stromal cells modify macrophage polarization for resolution of chronic inflammation via exosome-shuttled let-7b. *J Transl Med*. 2015;13:308. doi:10.1186/s12967-015-0642-6
59. Genin M, Clement F, Fattaccioli A, Raes M, Michiels C. M1 and M2 macrophages derived from THP-1 cells differentially modulate the response of cancer cells to etoposide. *BMC Cancer*. 2015;15:577. doi:10.1186/s12885-015-1546-9
60. Tedesco S, De Majo F, Kim J, et al. Convenience versus Biological Significance: are PMA-Differentiated THP-1 Cells a Reliable Substitute for Blood-Derived Macrophages When Studying Polarization? *Front Pharmacol*. 2018;9:71. doi:10.3389/fphar.2018.00071
61. Zhang D, Li X, Song D, et al. Atractylenolide III induces apoptosis by regulating the Bax/Bcl-2 signaling pathway in human colorectal cancer HCT-116 Cells in vitro and in vivo. *Anticancer Drugs*. 2022;33(1):30–47. doi:10.1097/CAD.0000000000001136
62. Cahyadi A, Ugrasena IDG, Andarsini MR, Larasati MCS, Aryati A, Arumsari DK. Relationship between Bax and Bcl-2 Protein Expression and Outcome of Induction Phase Chemotherapy in Pediatric Acute Lymphoblastic Leukemia. *Asian Pac J Cancer Prev*. 2022;23(5):1679–1685. doi:10.31557/APJCP.2022.23.5.1679
63. Ahmadian E, Eftekhari A, Kavetskyy T, Khosroushahi AY, Turksoy VA, Khalilov R. Effects of quercetin loaded nanostructured lipid carriers on the paraquat-induced toxicity in human lymphocytes. *Pestic Biochem Physiol*. 2020;167:104586. doi:10.1016/j.pestbp.2020.104586
64. Ahmadian E, Khosroushahi AY, Eftekhari A, Farajnia S, Babaei H, Eghbal MA. Novel angiotensin receptor blocker, azilsartan induces oxidative stress and NFkB-mediated apoptosis in hepatocellular carcinoma cell line HepG2. *Biomed Pharmacother*. 2018;99:939–946. doi:10.1016/j.biopha.2018.01.117
65. Lin C-W, Hung C-M, Chen W-J, et al. New Horizons of Macrophage Immunomodulation in the Healing of Diabetic Foot Ulcers. *Pharmaceutics*. 2022;14:10. doi:10.3390/pharmaceutics14102065
66. Deng L, Du C, Song P, et al. The Role of Oxidative Stress and Antioxidants in Diabetic Wound Healing. *Oxid Med Cell Longev*. 2021;2021:8852759. doi:10.1155/2021/8852759
67. Hasanzadeh A, Gholipour B, Rostamnia S, et al. Biosynthesis of AgNPs onto the urea-based periodic mesoporous organosilica (AgxNPs/Ur-PMO) for antibacterial and cell viability assay. *J Colloid Interface Sci*. 2021;585:676–683. doi:10.1016/j.jcis.2020.10.047
68. Sun B, Wu F, Wang X, et al. An Optimally Designed Engineering Exosome-Reductive COF Integrated Nanoagent for Synergistically Enhanced Diabetic Fester Wound Healing. *Small*. 2022;18(26):e2200895. doi:10.1002/smll.202200895
69. Bhatti JS, Bhatti GK, Reddy PH. Mitochondrial dysfunction and oxidative stress in metabolic disorders - A step towards mitochondria based therapeutic strategies. *Biochim Biophys Acta Mol Basis Dis*. 2017;1863(5):1066–1077. doi:10.1016/j.bbadis.2016.11.010
70. Zhao M, Liu S, Wang C, et al. Mesenchymal Stem Cell-Derived Extracellular Vesicles Attenuate Mitochondrial Damage and Inflammation by Stabilizing Mitochondrial DNA. *ACS Nano*. 2021;15(1):1519–1538. doi:10.1021/acsnano.0c08947
71. He Z-Y, Huang M-T, Cui X, et al. Long noncoding RNA GAS5 accelerates diabetic wound healing and promotes lymphangiogenesis via miR-217/Prox1 axis. *Mol Cell Endocrinol*. 2021;532:111283. doi:10.1016/j.mce.2021.111283
72. Pi L, Fang B, Meng X, Qian L. LncRNA XIST accelerates burn wound healing by promoting M2 macrophage polarization through targeting IL-33 via miR-19b. *Cell Death Discovery*. 2022;8(1):220. doi:10.1038/s41420-022-00990-x
73. Hanayama R, Tanaka M, Miwa K, Shinohara A, Iwamatsu A, Nagata S. Identification of a factor that links apoptotic cells to phagocytes. *Nature*. 2002;417(6885):182–187. doi:10.1038/417182a
74. Laplante P, Brillant-Marquis F, Brissette M-J, et al. MFG-E8 Reprogramming of Macrophages Promotes Wound Healing by Increased bFGF Production and Fibroblast Functions. *J Invest Dermatol*. 2017;137(9):2005–2013. doi:10.1016/j.jid.2017.04.030
75. Wang B, Ge Z, Wu Y, et al. MFGE8 is down-regulated in cardiac fibrosis and attenuates endothelial-mesenchymal transition through Smad2/3-Snail signalling pathway. *J Cell Mol Med*. 2020;24(21):12799–12812. doi:10.1111/jcmm.15871
76. Ge Z, Chen Y, Wang B, et al. MFGE8 attenuates Ang-II-induced atrial fibrosis and vulnerability to atrial fibrillation through inhibition of TGF-β1/Smad2/3 pathway. *J Mol Cell Cardiol*. 2020;139:164–175. doi:10.1016/j.yjmcc.2020.01.001
77. Xiaojie W, Banda J, Qi H, et al. Scarless wound healing: current insights from the perspectives of TGF-β, KGF-1, and KGF-2. *Cytokine Growth Factor Rev*. 2022;66:26–37. doi:10.1016/j.cytogfr.2022.03.001
78. Walton KL, Johnson KE, Harrison CA. Targeting TGF-β Mediated SMAD Signaling for the Prevention of Fibrosis. *Front Pharmacol*. 2017;8:461. doi:10.3389/fphar.2017.00461
79. Penn JW, Grobbelaar AO, Rolfe KJ. The role of the TGF-β family in wound healing, burns and scarring: a review. *Int J Burns Trauma*. 2012;2(1):18–28.

80. Hu -H-H, Chen D-Q, Wang Y-N, et al. New insights into TGF-β/Smad signaling in tissue fibrosis. *Chem Biol Interact*. 2018;292:76–83. doi:10.1016/j.cbi.2018.07.008
81. Huhn EA, Jannowitz C, Boos H, et al. Fetale Wundheilung Aktueller Stand und neue Perspektiven [Fetal wound healing: current status and new perspectives]. *Der Chirurg Zeitschrift Fur Alle Gebiete Der Operativen Medizen*. 2004;75(5):498–507. German. doi:10.1007/s00104-004-0878-9
82. Chen W, Fu X, Ge S, et al. Ontogeny of expression of transforming growth factor-beta and its receptors and their possible relationship with scarless healing in human fetal skin. *Wound Repair Regeneration*. 2005;13(1):68–75. doi:10.1111/j.1067-1927.2005.130109.x
83. Xie JL, Qi SH, Pan S, et al. Expression of Smad protein by normal skin fibroblasts and hypertrophic scar fibroblasts in response to transforming growth factor beta1. *Dermatol Surg*. 2008;34(9):1216–1225. doi:10.1097/00042728-200809000-00008
84. Jiang T, Wang Z, Sun J. Human bone marrow mesenchymal stem cell-derived exosomes stimulate cutaneous wound healing mediates through TGF-β/Smad signaling pathway. *Stem Cell Res Therapy*. 2020;11(1):198. doi:10.1186/s13287-020-01723-6